

Review

# Design Principles and Development Status of Flexible Integrated Thin and Lightweight Zinc-Ion Batteries

Xuxian Liu <sup>1</sup>, Yongchang Jiang <sup>2</sup>, Yaqun Wang <sup>1,2,\*</sup> and Lijia Pan <sup>2,\*</sup> 

<sup>1</sup> College of Energy Storage Technology, Shandong University of Science and Technology, Qingdao 266590, China; 202283080127@sdu.edu.cn

<sup>2</sup> School of Electronic Science and Engineering, Collaborative Innovation Center of Advanced Microstructures, Nanjing University, Nanjing 210093, China; ycjiang@nju.edu.cn

\* Correspondence: yqwang@sdu.edu.cn (Y.W.); lpan@nju.edu.cn (L.P.)

**Abstract:** The rapid advancement of wearable devices and flexible electronics has spurred an increasing need for high-performance, thin, lightweight, and flexible energy storage devices. In particular, thin and lightweight zinc-ion batteries require battery materials that possess exceptional flexibility and mechanical stability to accommodate complex deformations often encountered in flexible device applications. Moreover, the development of compact and thin battery structures is essential to minimize the overall size and weight while maintaining excellent electrochemical performance, including high energy density, long cycle life, and stable charge/discharge characteristics, to ensure their versatility across various applications. Researchers have made significant strides in enhancing the battery's performance by optimizing crucial components such as electrode materials, electrolytes, separators, and battery structure. This review provides a comprehensive analysis of the design principles essential for achieving thinness in zinc-ion batteries, along with a summary of the preparation methods and potential applications of these batteries. Moreover, it delves into the challenges associated with achieving thinness in zinc-ion batteries and proposes effective countermeasures to address these hurdles. This review concludes by offering insights into future developments in this field, underscoring the continual advancements and innovations that can be expected.



**Citation:** Liu, X.; Jiang, Y.; Wang, Y.; Pan, L. Design Principles and Development Status of Flexible Integrated Thin and Lightweight Zinc-Ion Batteries. *Batteries* **2024**, *10*, 200. <https://doi.org/10.3390/batteries10060200>

Academic Editor: Dino Tonti

Received: 10 May 2024

Revised: 5 June 2024

Accepted: 7 June 2024

Published: 10 June 2024



**Copyright:** © 2024 by the authors. Licensee MDPI, Basel, Switzerland. This article is an open access article distributed under the terms and conditions of the Creative Commons Attribution (CC BY) license (<https://creativecommons.org/licenses/by/4.0/>).

## 1. Introduction

Aqueous zinc-ion batteries are a promising energy storage solution that utilizes aqueous electrolytes and cost-effective, environmentally friendly zinc as negative electrodes. This technology offers significant advantages in terms of cost-effectiveness, environmental sustainability, and overall performance [1,2]. Zinc-ion batteries have a wide range of applications in energy storage, mobile power, and wearable electronic devices [3–7]. Among these applications, wearable devices stand out due to the rapid advancement of technology and the trend towards lighter and thinner electronic devices. The demand for batteries that are thin, lightweight, efficient, and environmentally friendly has never been greater. As a result, the research and development of zinc-ion batteries with a slim and compact design are of paramount importance in meeting these evolving needs.

The compact size and lightweight nature of thin zinc-ion batteries present a significant advantage, achieved through the utilization of advanced materials and design principles. This feature holds immense potential for integration into portable electronic devices, wearables, and various other applications. For example, in smartphones, tablets, and smartwatches, these lightweight batteries can provide extended battery life without increasing the overall size and weight of the device, thereby enhancing the user experience. The thickness of the thin and light zinc-ion batteries is tailored to suit the specific usage scenarios of wearable devices. Typically, each component of these batteries does not exceed

one millimeter in thickness and several hundred milligrams in weight, enabling the wearable device to operate without being hindered by battery mass. Moreover, the flexibility of the thin and light zinc-ion battery is crucial for meeting the demands of wearable technology. Flexible batteries can be bent or stretched, ensuring that they remain undamaged by deformation during use. Additionally, lightweight batteries are known for their environmentally friendly nature and high level of safety [8]. By utilizing zinc-ion batteries, the need for toxic substances commonly found in traditional battery chemistries is eliminated, resulting in a reduction in environmental pollution. Furthermore, the unique material composition and chemical properties of zinc-ion batteries help to mitigate potential safety hazards such as short-circuits or combustion incidents during charging and discharging processes, thereby enhancing overall battery safety. Nevertheless, the adoption of thin zinc-ion batteries presents a challenge in achieving high energy density due to the reduced content of active material [9–11]. Therefore, a key focus should be placed on the rational selection of materials and the design of the battery structure to enhance energy density. Additionally, ensuring outstanding cycle performance is essential [12,13] in the development of thin and lightweight zinc-ion batteries. In the realm of research and development for thin and lightweight zinc-ion batteries, there are five fundamental research directions that merit attention. These include optimizing the design of a thin and lightweight zinc cathode, anode, electrolyte, and separator and designing a compact and integrated battery structure. These design considerations not only significantly impact the overall performance of the battery but also have a direct influence on its practical applications:

- (A) The design of the zinc anode aims to achieve a slender and lightweight anode by optimizing the material, structure, and manufacturing process. This involves a careful balance between reducing size and weight while also maintaining or enhancing the energy density and cycle life of the battery.
- (B) The design of cathode materials should prioritize selecting those with high energy density to guarantee excellent battery performance, even in slim and lightweight conditions.
- (C) The design of separators should focus on developing thin and lightweight separators for liquid electrolytes that exhibit high ionic conductivity, strong electrochemical properties, and excellent mechanical characteristics.
- (D) The design of gels can be categorized into non-in situ-polymerized gels and in situ-polymerized gels, which help in reducing the size of the battery and enhancing its electrochemical performance.
- (E) The design of a streamlined battery structure entails organizing, connecting, and packaging internal components to create a highly integrated, compact, and lightweight battery that can cater to various application scenarios.

This review aims to comprehensively analyze the current research progress, challenges, and future development trends of thin and lightweight zinc-ion batteries from five perspectives: the design of thin and lightweight zinc anodes, cathode materials, electrolytes, and separators and the design of battery structures. By comparing various design schemes in terms of their advantages and disadvantages, this review seeks to uncover underlying connections and principles, providing theoretical support and practical guidance for the research, development, and application of thin and lightweight zinc-ion batteries (Figure 1).

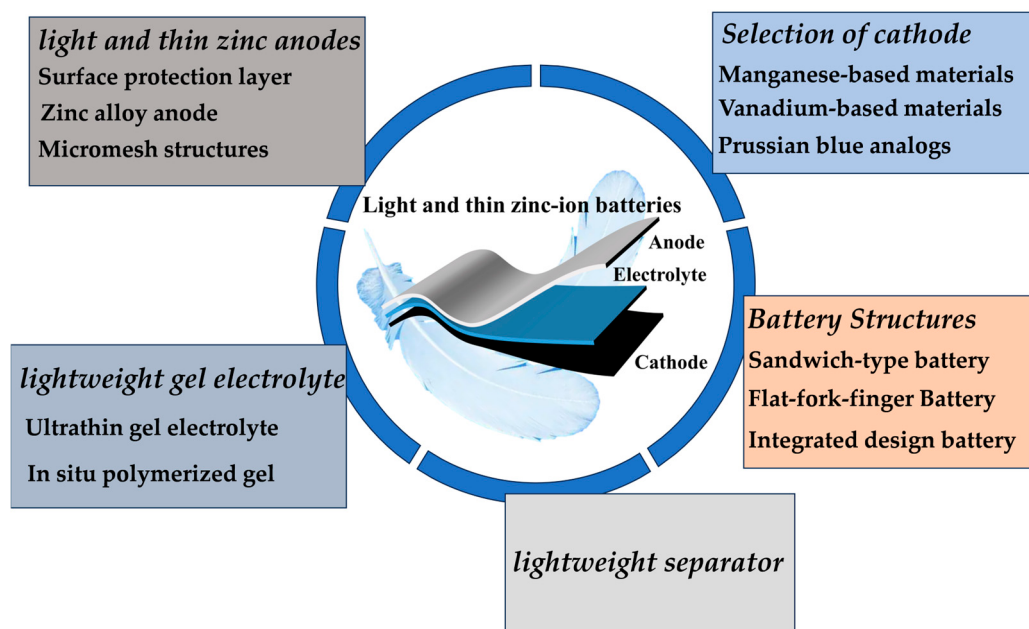


**Figure 1.** Schematic illustration of the design principles of a lightweight zinc-ion battery.

## 2. Design of Thin and Light Zinc Anodes

The development of lightweight and thin zinc-ion battery systems requires the utilization of lightweight, high-performance, and stretchable zinc anodes while ensuring proper functionality [14]. To achieve thin and lightweight zinc anodes, it is imperative to reduce their size and mass. Conventional thick zinc foil used as the negative electrode in zinc batteries often results in low energy density and increased battery costs, as well as larger and heavier battery sizes due to excessive negative electrode material [15–18]. Therefore, reducing the thickness of the zinc anode not only decreases the weight and size of the battery but also enhances the utilization rate of zinc batteries. The utilization rate of the zinc anode is typically determined using a depth of discharge (DOD) formula [14,19]. The DOD represents the percentage of the capacity involved in the electrode reaction compared to the overall capacity of the zinc metal anode:

$$DOD = \frac{C_{Zn,reactive}}{C_{Zn,overall}} \times 100\% \quad (1)$$

The DOD is indeed a critical parameter that provides insight into the zinc utilization and the performance of the Zn metal anodes in practical applications. It also serves as a key criterion for objectively assessing the performance of aqueous zinc-ion batteries (AZIBs). Consequently, according to Equation (1), reducing the quantity of zinc utilized in the anode emerges as an effective approach to enhance zinc utilization. However, the utilization of thick zinc foils often leads to low DOD levels due to the excessive zinc content, resulting in restricted available zinc and decreased energy density in fully assembled cells [20]. Therefore, reducing the volumetric mass by thinning the zinc foil represents a promising strategy. Nonetheless, this strategy presents inherent challenges such as interfacial failure, zinc corrosion, and unstable performance stemming from inadequate zinc reserves and the mechanical properties of thin and lightweight zinc foils. These challenges are commonly addressed through the construction of surface protection layers, the deposition of metal alloy layers on zinc foils, and the optimization of micro-network structures.

### 2.1. Surface Protection Layer

Due to the low zinc content of thin zinc anodes, the interface is susceptible to “tip reactions” during zinc deposition and dissolution, leading to the increased accumulation of “dead zinc” and hindering the efficient utilization of zinc. Dead zinc is inactive zinc

that will not participate in the reaction but will affect the battery performance. By incorporating a carefully designed interface layer, we can not only enhance the utilization efficiency of zinc foil but also mitigate dendrite formation, hydrogen precipitation, and corrosive reactions [21,22]. The design of the interface layer for thin zinc anodes necessitates careful consideration of material selection and design optimization, as well as ensuring appropriate thickness.

Hao implemented a gas–solid strategy to *in situ* construct a robust and homogeneous ZnS interface on the Zn surface, thereby significantly enhancing the reversibility of Zn (Figure 2a) [23]. The thickness of the ZnS film can be precisely controlled by adjusting the processing temperature, resulting in the formation of a dense protective layer with a mere thickness of 0.5  $\mu\text{m}$  at 350 °C (Figure 2b). This ZnS protective layer not only acts as a physical barrier against Zn corrosion but also effectively suppresses dendrite growth by guiding the plating/peeling process beneath it. As a result, ZnS@Zn symmetric batteries exhibit reduced polarization voltage and an extended cycle life of up to 1100 h. Furthermore, when assembled with MnO<sub>2</sub>, the full cell demonstrates exceptional cycling performance with an impressive capacity retention rate of 87.6% after undergoing 2500 cycles.

Ling successfully achieved a 50% increase in zinc utilization by fabricating an ion-screen interfacial protection (ZnSnF@Zn) directly on the surface of a zinc anode (Figure 2c), capitalizing not only on its heterogeneous structure but also exploiting the unique functionality of ZnSnF [24]. This interfacial layer facilitates the transport and desolvation process of zinc ions at the interface, thereby mitigating overpotential for zinc deposition and effectively suppressing undesired side reactions. Simultaneously, zinc metal can be deposited in a highly reversible and dense manner beneath the ionic sieve layer, ensuring efficient deposition efficiency and cyclic stability even for extremely thin zinc foils (Figure 2d). Experimental results demonstrate that the symmetric cell utilizing ZnSnF@Zn achieves stable cycling of up to 250 h at a current density of 30 mA  $\text{cm}^{-2}$  under conditions of 50% zinc utilization (Figure 2e). This result fully illustrates the remarkable effect of this interfacial protective layer in improving zinc foil utilization and enhancing cell performance.

Zhou utilized the unique dielectric properties of amorphous and nanostructured silicon nitride (Si<sub>3</sub>N<sub>4</sub>) to manipulate ionic dynamics by uniformly dispersing its particles in polyacrylonitrile (PAN) for the fabrication of a zinc metal-attached interlayer (PSN-Zn) (Figure 2f) [25]. The PAN, possessing exceptional mechanical properties, serves as an elastic confinement and barrier layer against H<sub>2</sub>O/O<sub>2</sub>, while the amorphous Si<sub>3</sub>N<sub>4</sub> nanoparticles with specialized dielectric characteristics regulate Zn electrodeposition behavior by controlling ionic distribution under an external electric field. With this protective layer, a mere 30  $\mu\text{m}$  thick Zn anode can sustain high current densities for up to 250 h at a depth of discharge (DOD) of 60%.

In addition to the protective layer formed by the inorganic compound, the porous structure of carbon material provides ample space for zinc deposition dissolution, thereby facilitating a more uniform diffusion of zinc ions through the carbon material protective layer. However, the binding of graphene to zinc is suboptimal. To address this issue, Zhou synthesized a nitrogen-doped graphene oxide (NGO) interfacial film using the Langmuir–Blodgett method in a single step, which provides protection for approximately 120 nm (Figure 3a) [26]. The parallel layers of graphene and nitrogen-doped groups exhibit favorable zincophilic properties, resulting in the directional deposition of zinc crystals along the (002) plane (Figure 3a). Moreover, the oriented plating morphology of metallic zinc at the interface effectively suppresses the hydrogen evolution reaction (HER) and passivation, as confirmed by *in situ* differential electrochemical mass spectrometry and *in situ* Raman tests. The symmetric cell assembled with NGO@Zn demonstrates excellent cyclability with 300 cycles at a current density of 5 mA  $\text{cm}^{-2}$  (Figure 3b). Furthermore, when paired with a LiMn<sub>2</sub>O<sub>4</sub> cathode, this Zn anode maintains outstanding energy density (164 Wh  $\text{kg}^{-1}$  after 178 cycles) at a depth of discharge (36% DOD) for soft pack batteries.

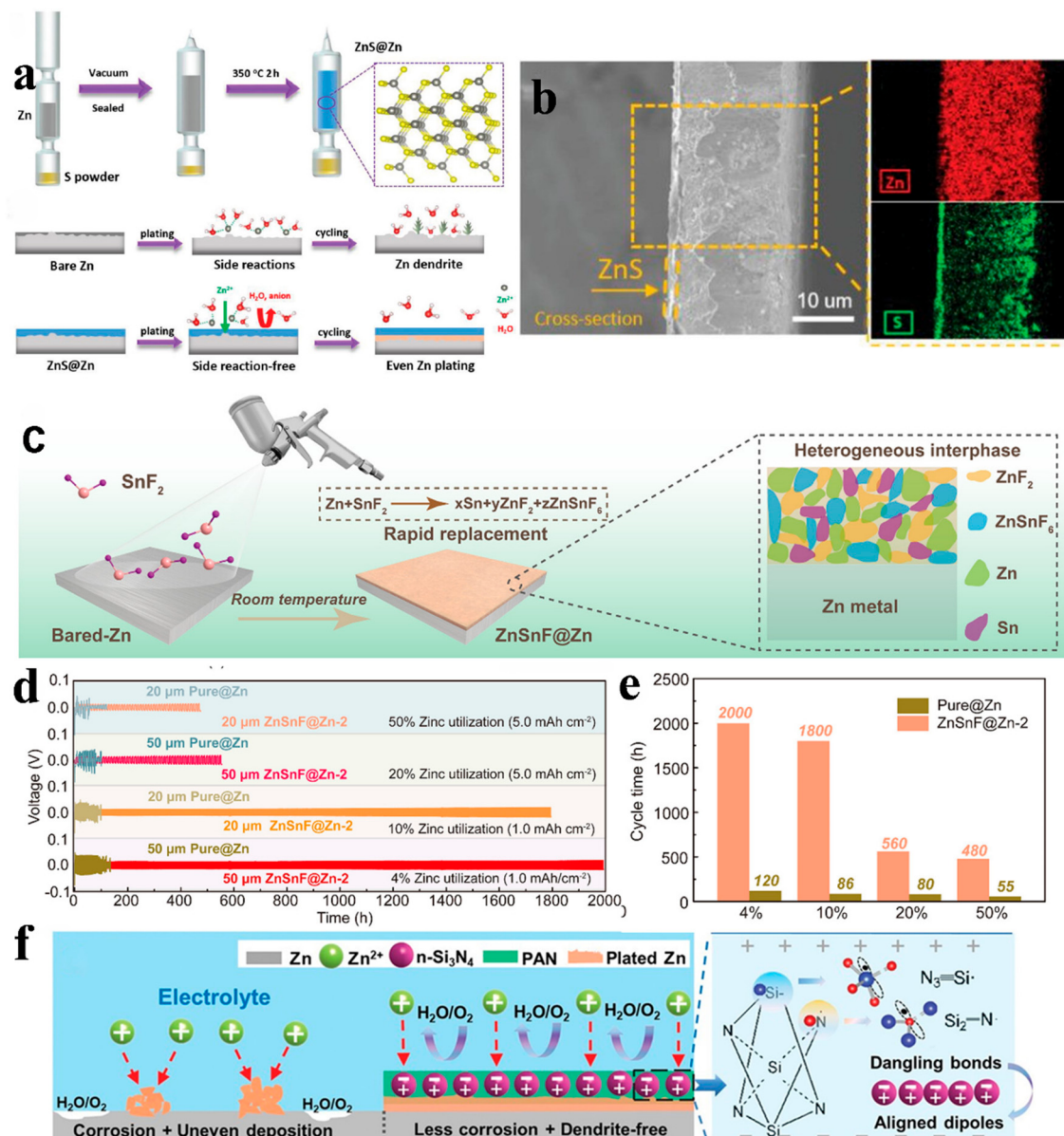


**Figure 2.** (a) Schematic illustration of the artificial ZnS layer and Zn plating behavior with/without ZnS. (b) Cross-sectional image of ZnS@Zn-350 foil, showing that the thickness of the ZnS is  $\approx 0.5 \mu\text{m}$ . EDS mapping of Zn element (**top**) and S element (**bottom**). Reprinted with permission from ref. [23]. Copyright 2024, American Chemical Society. (c) Schematic diagram of ion sieve interfacial layer formation on a zinc metal anode. (d) Galvanostatic cycling performance and (e) cycling lives of symmetric Zn||Zn batteries with Pure@Zn and ZnSnF@Zn-2 under various zinc utilizations. Reprinted with permission from ref. [24]. Copyright 2020, John Wiley and Sons. (f) Schematic illustration of Zn plating/stripping behavior on bare Zn (**left** panel) and Zn with PSN coating (**middle** panel). The **right** panel shows that the amorphous Si<sub>3</sub>N<sub>4</sub> nanoparticles exhibit novel dielectric behavior. Reprinted with permission from ref. [25]. Copyright 2021, John Wiley and Sons.

In addition to graphene, carbon nanotubes (CNTs) facilitate the enrichment of charge carriers and serve as an ideal protective layer for enhancing electric field distribution. Zhou employed a Zn-friendly CNT as a safeguard for the Zn foil, effectively refining the Zn<sup>2+</sup> carriers and electric field, with this protective layer being approximately 20  $\mu\text{m}$  thick (Figure 3c) [27]. The hydrophilicized CNT can permeate through a foam-like structure characterized by abundant porosity. Consequently, the CNT protective layer becomes an exceptional medium conducive to Zn<sup>2+</sup> carrier transport, facilitating substantial transfer

of  $Zn^{2+}$  ions and thereby promoting their transferability. Moreover, owing to its relatively lower conductivity compared to metallic zinc, the CNT protective layer enables bottom-up zinc deposition. Additionally, capacitive interfacial processes further enhance zinc deposition kinetics in bilayer form at the interface between CNTs and zinc metal (Figure 3d). The symmetric cell demonstrates stable cycling performance over 1000 cycles at a current density of  $50 \text{ mA cm}^{-2}$  while retaining good capacity in assembled  $MnO_2$  full cells. However, apart from meeting performance requirements, simplicity in the preparation process is also crucially considered.

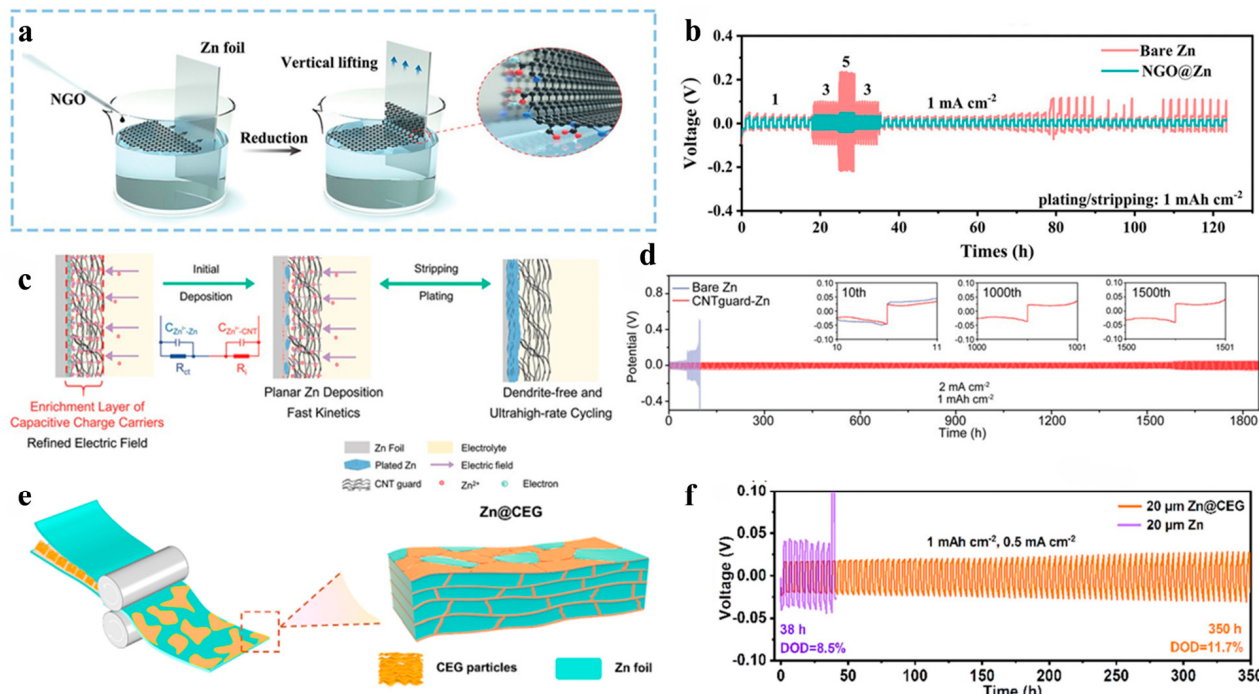


**Figure 3.** (a) Schematic illustration of fabricating ultrathin graphene layers on the Zn foil. (b) Rate performance at a fixed capacity of  $1 \text{ mAh cm}^{-2}$ . Reprinted with permission from ref. [26]. Copyright 2021, John Wiley and Sons. (c) Uneven dendrite formation on a bare Zn and dendrite-free zinc deposition on CNTguard-Zn during the Zn stripping/plating cycling. (d) Galvanostatic cycling of symmetric bare Zn and CNTguard-Zn cells at  $2 \text{ mA cm}^{-2}$  and  $1 \text{ mAh cm}^{-2}$  (insets: the charge/discharge curves at the 10th, 1000th, and 1500th cycles). Reprinted with permission from ref. [27]. Copyright 2023, John Wiley and Sons. (e) Schematic diagram of a Zn@CEG composite foil prepared by room temperature rolling. (f) Cycling performance of  $20 \mu\text{m}$  ultrathin electrodes at  $1 \text{ mAh cm}^{-2}$  and  $0.5 \text{ mA cm}^{-2}$ . Reprinted with permission from ref. [28]. Copyright 2023, Elsevier.

To simplify the preparation process of thin and lightweight zinc anodes, Meng proposed a strategy for preparing ultrathin zinc–carbon composite anodes (Zn@CEG) through room-temperature co-roll pressing of commercially available zinc foil with expanded graphite (CEG) (Figure 3e) [28]. By precisely controlling the thickness of the composite anode, ultrathickness ranging from  $40 \mu\text{m}$  to  $20 \mu\text{m}$  and even down to  $6 \mu\text{m}$  was achieved. The incorporation of CEG as the main framework in the Zn@CEG composite anode not only simplifies the preparation process and reduces costs but also ensures uniformity and stability due to its excellent film-forming property. The island-like distribution of CEG on the anode surface creates hydrophobic micro-regions that efficiently accelerate the desolvation and transport processes of  $Zn^{2+}$ , thereby enhancing ion migration efficiency between the electrolyte and anode. Moreover, CEG enhances flatness during rolling, facilitating even surface current density distribution and guiding the uniform deposition of  $Zn^{2+}$  while effectively suppressing dendrite formation. Additionally, the three-dimensional interpenetrating network structure formed by CEG and zinc improves electrical conductivity while

promoting the enhanced utilization of zinc. This structure enables more uniform participation of zinc in charging/discharging processes, reducing unused “dead zinc” content, thus improving energy density and cycle performance (Figure 3f).

## 2.2. Zinc Alloy Anode

Due to the susceptibility of lightweight zinc anodes to damage during prolonged cycling, they cannot serve as a reliable substrate for zinc deposition dissolution. Therefore, constructing a zinc metal alloy anode using a suitable metal as a substrate is deemed as a viable strategy to ensure the stable cycling of thin and lightweight zinc batteries. Moreover, the utilization of zinc is enhanced by employing a zinc metal alloy, while simultaneously improving the electrical conductivity and mechanical strength of the zinc anode. Copper is a metal renowned for its exceptional mechanical properties, low resistivity, and high electrical conductivity. Furthermore, its mechanical properties are truly outstanding. Simultaneously, the low resistivity of copper ensures excellent electrical conductivity. In the case of the zinc–copper alloy, this particular alloy exhibits enhanced corrosion resistance owing to copper’s inherent electrochemical inertness and higher corrosion potential compared to zinc. Enhanced corrosion resistance holds immense significance for metal anodes, particularly in applications demanding superior performance, as it prolongs anode lifespan and mitigates performance degradation caused by corrosion [29,30]. Zinc–copper alloys amalgamate the finest attributes of both zinc and copper while excelling notably in terms of corrosion resistance, rendering them one of the most prevalent high-performance zinc alloy anodes.

Zhang proposes a synergistic approach to modify zinc anodes by combining a Cu-Zn solid solution interface on a copper mesh skeleton with excellent zinc affinity and incorporating a polyacrylamide electrolyte additive (Figure 4a) [31]. This method significantly reduces the overpotential for zinc nucleation and enhances the stability of zinc deposition, making it highly suitable for lightweight zinc-ion battery anodes (Figure 4b). Furthermore, the resulting zinc anode deposited on ultrathin and lightweight copper exhibits exceptional performance in terms of low-voltage cycling (93.1 mV) for over 280 h at 80% discharge depth in symmetric cells. Additionally, Zn//MnO<sub>2</sub> full cells demonstrate high capacity retention and low polarization. Additionally, Zhou provided further evidence of the advantages of zinc–copper alloys in zinc anodes through the electrochemical deposition of zinc onto the surface of Cu-Zn alloys (Cu-Zn) (Figure 4b) [32]. The presence of zincophilic Cu sites within these alloys plays a pivotal role by significantly enhancing Zn<sup>2+</sup> adsorption capacity and promoting the homogeneous nucleation of zinc on the alloy surface. Consequently, the incorporation of Cu-Zn alloys renders the process of zinc plating/stripping more reversible, thereby improving cell performance and longevity. Furthermore, the Cu-Zn alloys were found to exhibit inherent inertness towards HER and possess a high dezincification potential, as demonstrated through experimental investigations. HER is a common side reaction in water electrolytes that depletes active substances in the electrolyte and can lead to battery performance degradation. The hydrogen evolution inertness of Cu-Zn alloys helps minimize this side reaction, while their high dezincification potential enhances cell stability and durability. Consequently, symmetric cells with Cu-Zn lightweight electrodes demonstrate exceptional cycle life in both alkaline and neutral electrolytes, exhibiting stable operation for over 800 h and 1600 h at a current density of 2.5 mAh cm<sup>-2</sup>, respectively, surpassing the performance of original Zn electrodes. Li successfully developed an ultrathin Zn composite anode with a thickness of only 24 µm (Figure 4c,d) [33]. The lightweight and thin Zn anode is a (C<sub>2</sub>F<sub>4</sub>)<sub>n</sub>-C@Cu composite structure fabricated through one-step pyrolytic evaporation deposition on a copper foil. The repulsive force between (C<sub>2</sub>F<sub>4</sub>)<sub>n</sub> and Zn<sup>2+</sup> leads to enhanced adsorption capacity at the (C<sub>2</sub>F<sub>4</sub>)<sub>n</sub>-C@Cu interface, facilitating increased charge transfer within the layer. Moreover, owing to its excellent hydrophobicity, this layer effectively safeguards the galvanized layer against water damage. Based on these findings, the (C<sub>2</sub>F<sub>4</sub>)<sub>n</sub>-C@Cu@Zn symmetric cell demonstrates exceptional stability and cycling performance when operated at a current density of 5 mA cm<sup>-2</sup> and discharged to a depth of 40% (Figure 4e). Furthermore, in full-cell configuration, it exhibits remarkable

durability with 2500 cycles achieved at a current density of  $3\text{ A g}^{-1}$  while maintaining an impressive capacity retention rate of 88.35%.

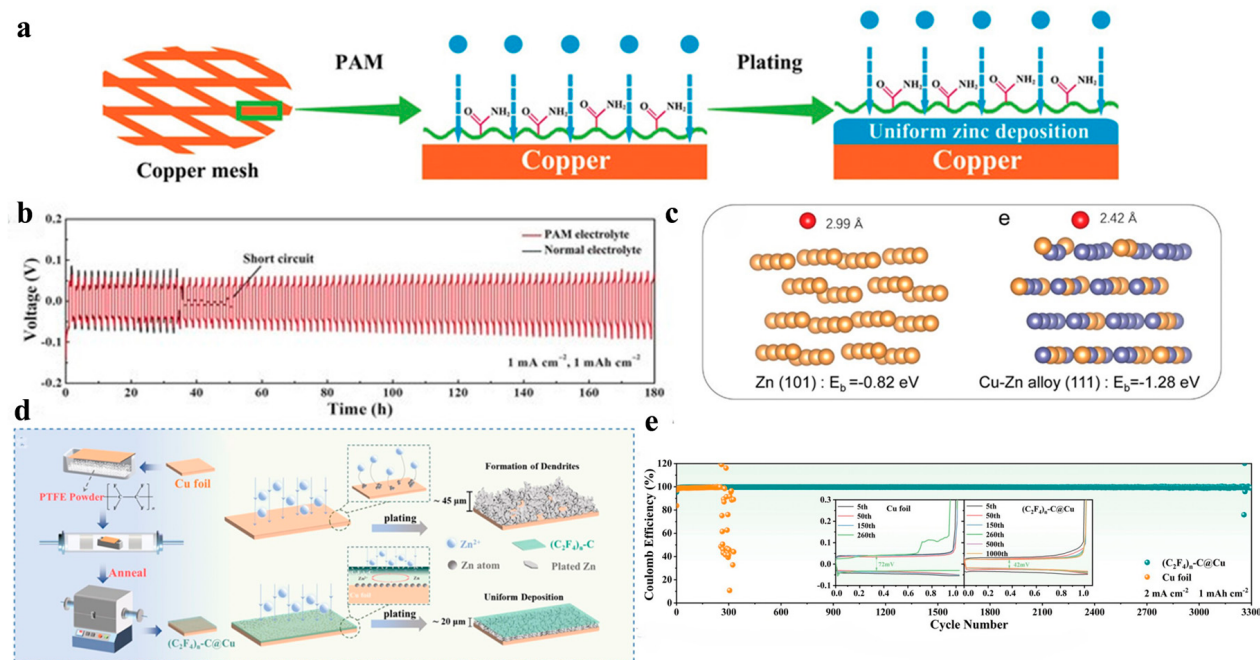


**Figure 4.** (a) Illustration of zinc deposition on the copper mesh in PAM-added electrolytes. (b) Cycling performance in symmetric cells and the corresponding voltage profiles in the 10th cycle at  $1\text{ mA cm}^{-2}$  for  $1\text{ mAh cm}^{-2}$ . Reprinted with permission from ref. [31]. Copyright 2019, John Wiley and Sons. (c) The calculated binding energy of  $\text{Zn}^{2+}$  on Zn (101) and Cu-Zn alloy (111). Reprinted with permission from ref. [32]. Copyright 2021, John Wiley and Sons. (d) The schematic diagram of the preparation of the  $(\text{C}_2\text{F}_4)_n\text{-C}@\text{Cu}$  substrate. (e) CE of Zn plating/stripping on  $(\text{C}_2\text{F}_4)_n\text{-C}@\text{Cu}$  and Cu foil at  $2\text{ mA cm}^{-2}$  and  $1\text{ mAh cm}^{-2}$  (inset is selected voltage profiles). Reprinted with permission from ref. [33]. Copyright 2023, John Wiley and Sons.

### 2.3. Designing Lightweight Micromesh Structures for Zinc Anodes

Compared to planar zinc foils, the micromesh structure of zinc anode design offers exceptional flexibility and mechanical strength while increasing the contact area with the electrolyte. Moreover, this micromesh structure facilitates uniform ion concentration and orderly distribution of the electric field, promoting preferential nucleation and dendrite-free deposition of  $\text{Zn}^{2+}$  ions on the inner wall of micropores. By employing a combination of photolithography and electrochemical processing techniques, Liu successfully fabricates a flexible, ultrathin, and ultralight Zn microgrid with remarkable performance (Figure 5a) [34]. The micromesh exhibits exceptional flexibility, foldability, and enhanced mechanical strength due to its mere  $8\text{ }\mu\text{m}$  thickness and remarkably low surface density (Figure 5b,c). Its unique microporous design enables the Zn micromesh to possess superior wettability, a crucial factor in enhancing battery performance. As a Zn anode, this micro-network exhibits significant advantages over conventional planar Zn films. The precisely arranged microporous structure not only induces spatially selective deposition and effectively suppresses dendrite growth, thereby reducing the overpotential, but also enhances the cycling stability of the cell. The aqueous zinc-ion battery (ZIB) assembled with a polyaniline intercalated vanadium oxide (PVO) cathode and a Zn micromesh anode demonstrates exceptional high multiplicity capability and long-term stability.

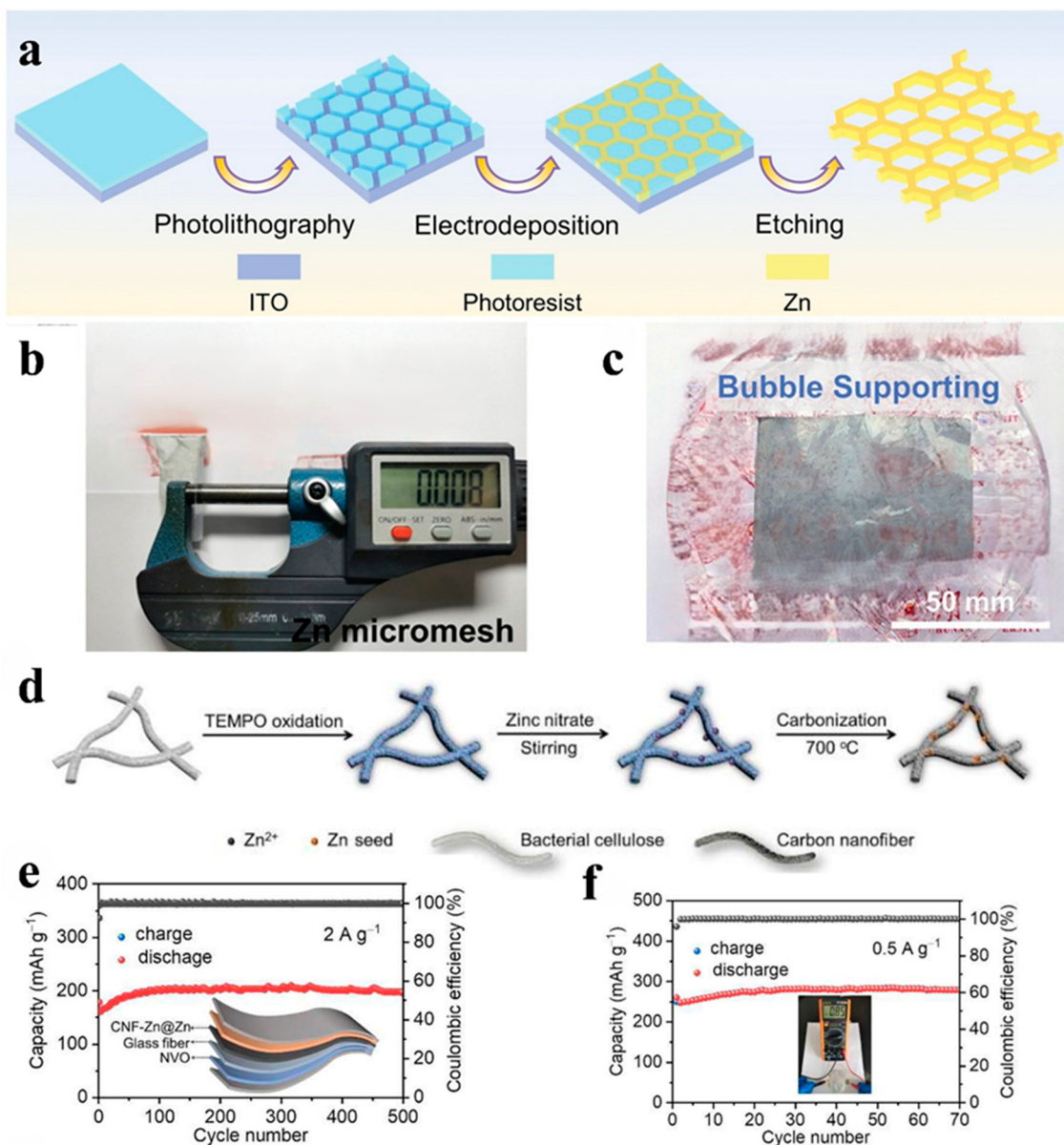


**Figure 5.** (a) Schematic showing the fabrication process flow of Zn micromesh. (b) Digital photo of the ultrathin Zn micromesh with a thickness of 8  $\mu\text{m}$ . (c) Digital photo of the ultralight Zn micromesh supported on bubbles. Reprinted with permission from ref. [34]. Copyright 2021, John Wiley and Sons. (d) Schematic diagram for the synthesis of CNF-Zn. Electrochemical performance of pouch cells using the CNF-Zn@Zn anode and NVO cathode. Cycling performance at different current densities: (e)  $2 \text{ A g}^{-1}$  and (f)  $0.5 \text{ A g}^{-1}$ . Reprinted with permission from ref. [35]. Copyright 2023, American Chemical Society.

Utilizing bacterial cellulose (BC) as a substrate, Wang fabricated lightweight and flexible 3D carbon nanofiber structures embedded with uniformly distributed zinc seeds (CNF-Zn) to serve as hosts for highly reversible zinc electrodeposition and the construction of high-performance aqueous ZIBs (Figure 5d) [35]. The interconnected porous network within the 3D CNF-Zn hosts significantly mitigates localized current density, while the functional zinc seeds facilitate uniform zinc deposition by providing homogeneous nuclei. The electrochemical performance of the developed ZIBs was substantially enhanced through the synergistic effect of the flexible 3D porous framework offered by the CNF-Zn host and incorporated zinc seeds, exhibiting exceptional stability with an electrochemical efficiency exceeding 99.5% over 450 cycles along with excellent multiplicity performance. More-

over, it demonstrated a prolonged lifetime surpassing 500 cycles in full-cell configuration (Figure 5e,f).

The design of thin and lightweight zinc anodes encompasses three key aspects: the surface treatment of the zinc, generation of zinc alloys, and design of the zinc micro-network. The surface treatment of the zinc is crucial for achieving optimal electrochemical properties in even the thinnest zinc foils. Additionally, the generation of zinc alloys provides a stable substrate for the deposition and dissolution processes of thin and lightweight zinc anodes over extended cycles, while also mitigating corrosion and other undesirable reactions in zinc cells. Furthermore, the design of a zinc micromesh serves to not only increase the contact area between the anode and electrolyte but also to enhance the mechanical strength of the zinc anode.

### 3. Selection of Cathode

The cathode material of lightweight zinc-ion batteries is a crucial component, comprising a uniform blend of zinc storage material, conductive additives, and binder, all co-coated onto the collector [36,37]. The zinc storage material typically consists of compounds with a favorable redox window, many of which possess a layered, framework, or tunnel structure. This cathode material serves as a host for storing  $Zn^{2+}$  ions, playing a significant role in determining the operating voltage and discharge specific capacity of the batteries. Therefore, the selection of high-quality cathode materials is essential to ensure excellent electrochemical performance, especially at low loadings. Due to the electrostatic interactions that occur during the insertion and extraction of zinc ions in cathode materials, it is imperative for these materials to exhibit characteristics such as high capacity and structural stability. Materials with tunneling structures and large layer spacings, such as manganese-based compounds, vanadium-based compounds, and Prussian blue analogs, have been extensively studied as cathode materials for aqueous zinc-ion batteries. These materials are capable of accommodating the zinc ions effectively, thereby enhancing the overall performance of the batteries.

#### 3.1. Manganese-Based Materials

Manganese-based materials are highly favored for their advantageous characteristics, including low toxicity, high voltage, high specific capacity, and cost-effectiveness [38]. As a result, manganese-based compounds have become prevalent choices for cathode materials in zinc-ion batteries. Due to the constraints imposed by the decomposition voltage of water, the selection of cathode compounds has been primarily focused on two oxidation states: +4 and +3. This includes compounds such as  $MnO_2$ ,  $Mn_2O_3$ , and  $Mn_3O_4$ , as well as spinel-phase compounds like  $ZnMn_2O_4$  and  $MgMn_2O_4$ .

Among these options,  $MnO_2$  stands out as the most prevalent choice, boasting the highest theoretical specific capacity of 308 mAh/g. Its widespread use in zinc-ion batteries is a testament to its exceptional electrochemical performance and compatibility with the requirements of the system. The versatility and efficiency of manganese-based materials make them indispensable components in the development of high-performance aqueous zinc-ion batteries. Nevertheless, manganese-based cathode materials are often plagued by challenges such as limited electronic conductivity, sluggish  $Zn^{2+}$  reaction kinetics, volume expansion during cycling, and the dissolution of cathode materials. These issues contribute to the rapid decay in specific capacity and the compromised cycling stability of the batteries, ultimately diminishing the overall applicability and value of manganese-based materials in battery systems.

Wu uniformly coated graphene spools onto  $MnO_2$  nanowires at an average width of 5 nm, thereby increasing the electrical conductivity of the  $MnO_2$  nanowires and alleviating the problem of dissolution of cathode materials during cycling. The assembled full battery achieved an energy density of  $406.6 \text{ Wh kg}^{-1}$  ( $382.2 \text{ mA h g}^{-1}$ ) at  $0.3 \text{ A g}^{-1}$  (Figure 6a,b) [39]. Ding implemented both defect engineering and interface optimization techniques on manganese oxide electrodes for AZIBs (Figure 6c,d) [40]. During the

preparation process, oxygen vacancies were naturally introduced in the  $\beta$ -MnO<sub>2</sub> through the presence of GO, resulting in a unique coating on the active material. For the prepared oxygen-deficient  $\beta$ -MnO<sub>2</sub>@GO cathode, manganese dissolution was significantly suppressed during electrochemical cycling, and the charge/discharge kinetics were greatly enhanced. The electrode maintains a high capacity of about 129.6 mAh g<sup>-1</sup> after 2000 cycles at a current rate of 4C, which is much better than the original  $\beta$ -MnO<sub>2</sub> electrode (Figure 6e). The excellent cycling stability is attributed to the strong bonding between the surface VO and the ether oxygen on the GO, as well as the ordered structural transition to the nanocrystalline ZnxMn<sub>2</sub>O<sub>4</sub> phase.

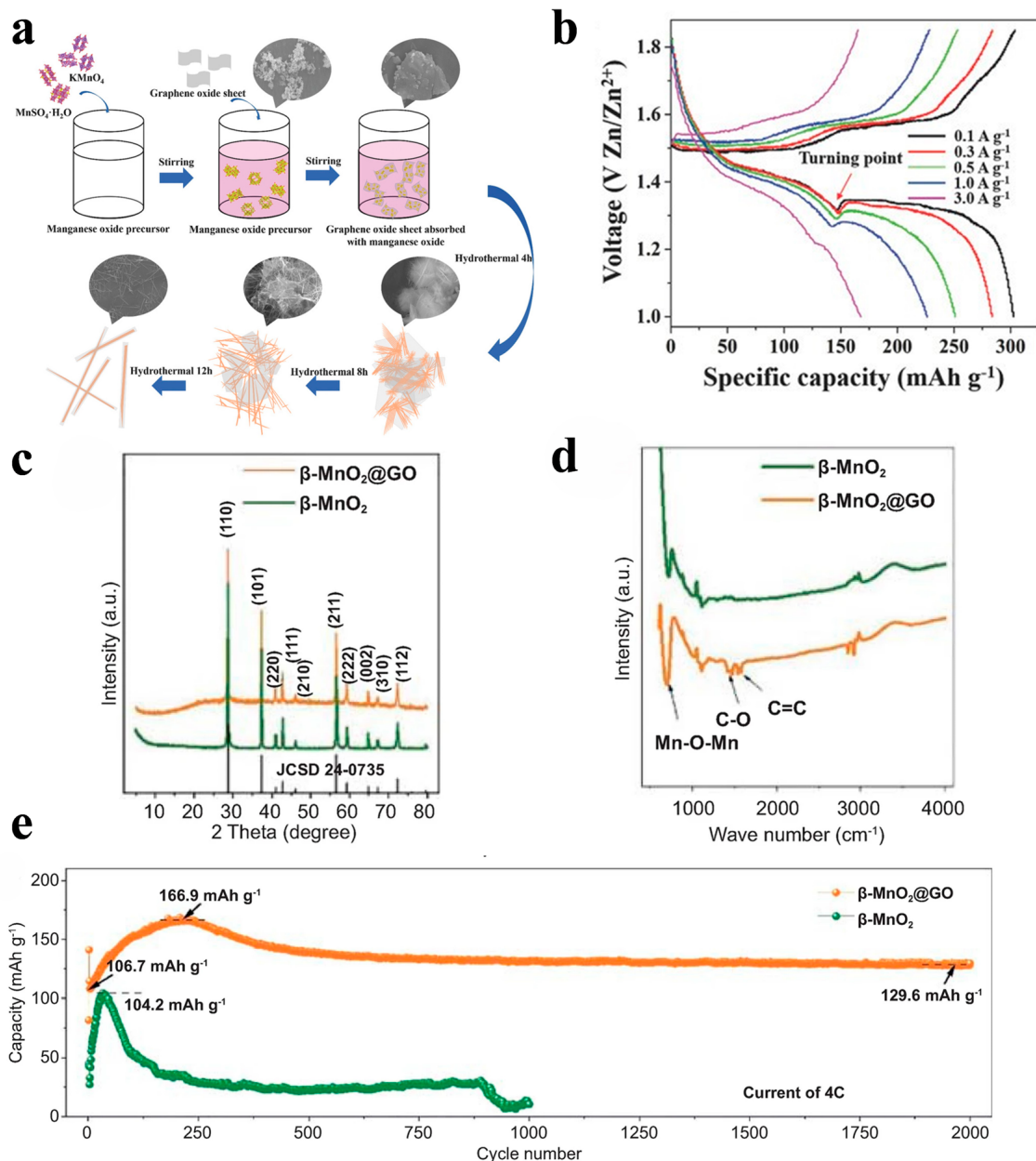


**Figure 6.** (a) Schematic illustration of the formation of the MGS. (b) Charge and discharge curves of MGS at current densities ranging from 0.1 to 3 A g<sup>-1</sup>. Reprinted with permission from ref. [39]. Copyright 2018, John Wiley and Sons. (c) XRD patterns of  $\beta$ -MnO<sub>2</sub> and  $\beta$ -MnO<sub>2</sub>@GO. (d) Comparison of FTIR spectra of  $\beta$ -MnO<sub>2</sub> and  $\beta$ -MnO<sub>2</sub>@GO. (e) Cycling performances of  $\beta$ -MnO<sub>2</sub> and  $\beta$ -MnO<sub>2</sub>@GO electrodes at the rate currents of 4C. Reprinted with permission from ref. [40]. Copyright 2021, Springer Nature.

### 3.2. Vanadium-Based Materials

Vanadium-based materials represent a promising class of anode materials for aqueous zinc-ion batteries [41]. The multivalent nature of vanadium enables multi-step redox reactions, leading to a high theoretical specific capacity. Additionally, these materials offer a favorable voltage platform typically ranging from 0.8 to 1.0 V (vs. Zn/Zn<sup>2+</sup>). The structural configuration, characterized by easily deformable V-O polyhedra interlinked with one another, provides vanadium-based materials with exceptional design flexibility. Presently, a diverse range of vanadium-based materials have been successfully utilized as cathode materials in aqueous zinc-ion batteries, including vanadium oxides (V<sub>2</sub>O<sub>5</sub>, VO<sub>2</sub>, V<sub>2</sub>O<sub>3</sub>, V<sub>6</sub>O<sub>13</sub>, etc.), vanadates (NaV<sub>3</sub>O<sub>8</sub>·1.5H<sub>2</sub>O, LiV<sub>3</sub>O<sub>8</sub>, CuV<sub>2</sub>O<sub>6</sub>, etc.), and vanadium-based materials with the structure of a polyanionic framework (NASICON). Additionally, other vanadium-based materials such as vanadium sulfides, vanadium–nitrogen oxides, and various oxides exhibit higher capacities compared to manganese-based compounds. However, they are characterized by lower discharge voltages. Moreover, vanadium-based cathode materials have problems such as high Zn<sup>2+</sup> diffusion resistance in the electrode, vanadium dissolution in aqueous electrolytes, and structural instability.

Gao designed and fabricated a cathode material (Figure 7a,b), 3D@V<sub>2</sub>O<sub>5</sub>, with a layered core–shell structure by combining fused deposition modeling (FDM) 3D printing technology with atomic layer deposition (ALD) [42]. In this innovative approach, a 3D-printed porous carbon network constitutes the core of the cathode, which not only provides efficient electron conduction channels but also builds interconnected ion diffusion pathways. The atomic layer deposition (ALD) technique, on the other hand, uniformly coats the carbon network with V<sub>2</sub>O<sub>5</sub> as the active shell, which enhances the electrochemical performance of the cathode while maintaining the porosity for Zn<sup>2+</sup> ion diffusion. Due to this unique structural design, the 3D@V<sub>2</sub>O<sub>5</sub> cathode exhibits excellent electrochemical performance. It possesses a high specific capacity (425 mAh g<sup>-1</sup> at a current density of 0.3 A g<sup>-1</sup>) along with competitive energy density and power density (316 Wh kg<sup>-1</sup> at a power density of 213 W kg<sup>-1</sup> and 163 Wh Kg<sup>-1</sup> at a power density of 3400 W kg<sup>-1</sup>) (Figure 7c,d). In addition, the cathode exhibits good rate performance with a specific capacity of 221 mAh g<sup>-1</sup> even at current densities up to 4.8 A g<sup>-1</sup>. Wang achieved three-dimensional ion diffusion in layered V<sub>2</sub>O<sub>5</sub> along the c-axis and ab-plane by opening the traffic in the basal plane [43]. A novel V<sub>2</sub>O<sub>5</sub> material (V<sub>2</sub>O<sub>5</sub>/C) with layered porous nanosheets grown vertically on carbon cloth was prepared by solvothermal and annealing processes. The uniformly arranged array of V<sub>2</sub>O<sub>5</sub> nanosheets effectively shortened the ion diffusion path. In addition, the porous structure with lattice defects provided additional ion diffusion channels and a large number of active sites along the c-axis, enabling an efficient 3D Li<sup>+</sup>/Zn<sup>2+</sup> co-insertion/extraction mechanism in the formulated 15 m LiTFSI + 1 m Zn(CF<sub>3</sub>SO<sub>3</sub>)<sub>2</sub> aqueous electrolyte. As a result, this customized cathode provided excellent rate performance (467.2 mAh g<sup>-1</sup> at 0.2 A g<sup>-1</sup> and 139.1 mAh g<sup>-1</sup> at 80 A g<sup>-1</sup>) (Figure 7e) and an ultra-long lifetime (90.7% capacity retention at 15,000 cycles) (Figure 7f) in RAZB. In addition, the Li<sup>+</sup>/Zn<sup>2+</sup> co-insertion chemistry greatly increases the energy density of porous V<sub>2</sub>O<sub>5</sub>/C by ≈58% compared to the Zn<sup>2+</sup>-only insertion behavior.

### 3.3. Prussian Blue Analogs

Prussian blue analogs are known for their capacity to act as host materials for a wide range of metal ions, with cubic metal–organic compounds exhibiting expansive embedded channels and high ionic conductivity [44]. Among these analogs, metal hexacyanoferrate (HCF) stands out as a particularly promising candidate due to its ability to serve as a host material for both monovalent and multivalent ions. In the context of aqueous zinc-ion batteries, the reversible embedding process of ZnHCF and CuHCF in ZnSO<sub>4</sub> electrolyte has been demonstrated, underscoring their potential for practical application.

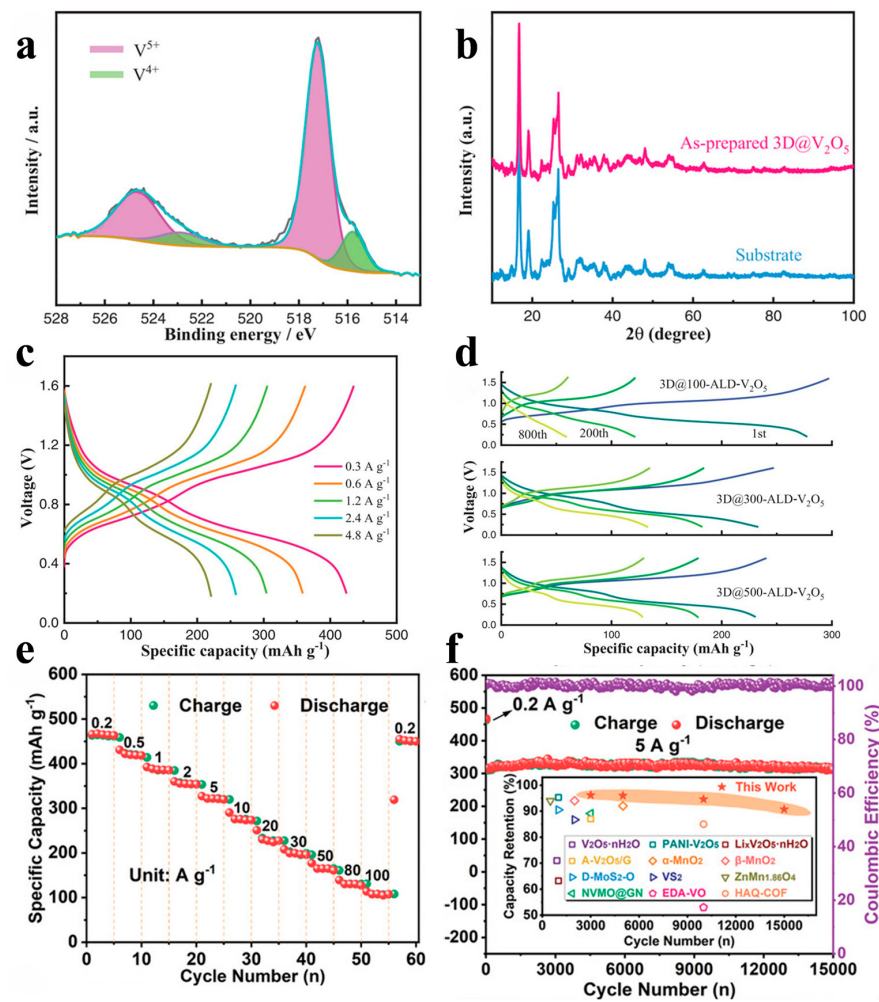


**Figure 7.** (a) V 2p XPS and (b) XRD spectra of as-prepared 3D@300-ALD-V<sub>2</sub>O<sub>5</sub> electrode. a.u., arbitrary units. (c) Discharge/charge profiles at various current densities. (d) Corresponding discharge/charge curves of 1st, 200th, and 800th cycles. Reprinted with permission from ref. [42]. Copyright 2021, John Wiley and Sons. (e) Rate performance at 0.2–100 A g<sup>-1</sup> of porous V<sub>2</sub>O<sub>5</sub>/C. (f) Long-term cycling performance of porous V<sub>2</sub>O<sub>5</sub>/C. Inset shows the comparison of capacity retention between this work and other reported aqueous Zn-storage cathodes. Reprinted with permission from ref. [43]. Copyright 2023, John Wiley and Sons.

Furthermore, Prussian blue analogs demonstrate a notably high anodic potential, approaching 1.7 V vs. Zn/Zn<sup>2+</sup> and aligning closely with the oxygen reduction reaction potential in aqueous electrolytes. This characteristic indicates good stability and compatibility with the electrolyte, showcasing their potential for use in advanced battery systems. However, it is important to note that despite their favorable electrochemical properties, all Prussian blue analogs exhibit a specific capacity of approximately 60 mAh g<sup>-1</sup>, which falls short of the capacities seen in manganese- and vanadium-based compounds. This discrepancy may impact the overall energy storage performance of Prussian blue analogs, highlighting an area for potential improvement and optimization in future research and development endeavors.

Prussian blue analogs exhibit a low specific capacity primarily attributed to inadequate material conductivity and a limited number of active sites. These factors contribute to a decrease in their energy density. Furthermore, the phase transition process that occurs within the electrodes during cycling leads to specific capacity decay and diminishes overall cycling performance. These challenges underscore the importance of addressing issues related to material conductivity, active site availability, and phase transition behavior to

enhance the specific capacity, energy density, and cycling performance of Prussian blue analogs in battery applications.

Yang epitaxialized iron on manganese hexacyanoferrate to construct core–shell diatomic redox Prussian blue analogs (PBAs) [45]. Upon ion insertion, the shell iron–Prussian blue analogs show minor volume changes that tend to surface amorphization, resulting in a low-strain core–bivalve structure. The in situ surface reorganization effectively suppressed the Jahn–Teller aberration and prevented manganese dissolution into the core–Mn-PBA electrolyte. As a result, this cathode design facilitates the realization of high-voltage full cells (more than 1.8 V for  $Zn^{2+}/Zn$ ) with high discharge capacities of up to  $166 \text{ mAh g}^{-1}$  and  $117 \text{ mAh g}^{-1}$  at  $0.1 \text{ A g}^{-1}$  and  $2 \text{ A g}^{-1}$  (Figure 8a), respectively, and capacity retention of 72.4% and 83.9% at 400 and 4800 cycles (Figure 8b), respectively. The pouch batteries can be successfully operated in harsh conditions from  $-30$  to  $60$  °C (Figure 8c). Zeng prepared Cu-substituted Mn-PBA double-shell nanoboxes (CuMn-PBA DSNBs) by tannic acid etching and cation exchange for efficient zinc-ion storage [46]. The unique hollow structure can expose abundant active sites and alleviate the volume change during cycling. In addition, partial Cu substitution and induced Mn vacancies may inhibit the Jahn–Teller aberration of the Mn-N<sub>6</sub> octahedron, thus contributing to the prolonged lifetime. As a result, the CuMn-PBA DSNBs exhibited high reversible capacity (Figure 8d), good rate performance, and superior cycling stability for 2000 cycles (Figure 8e).

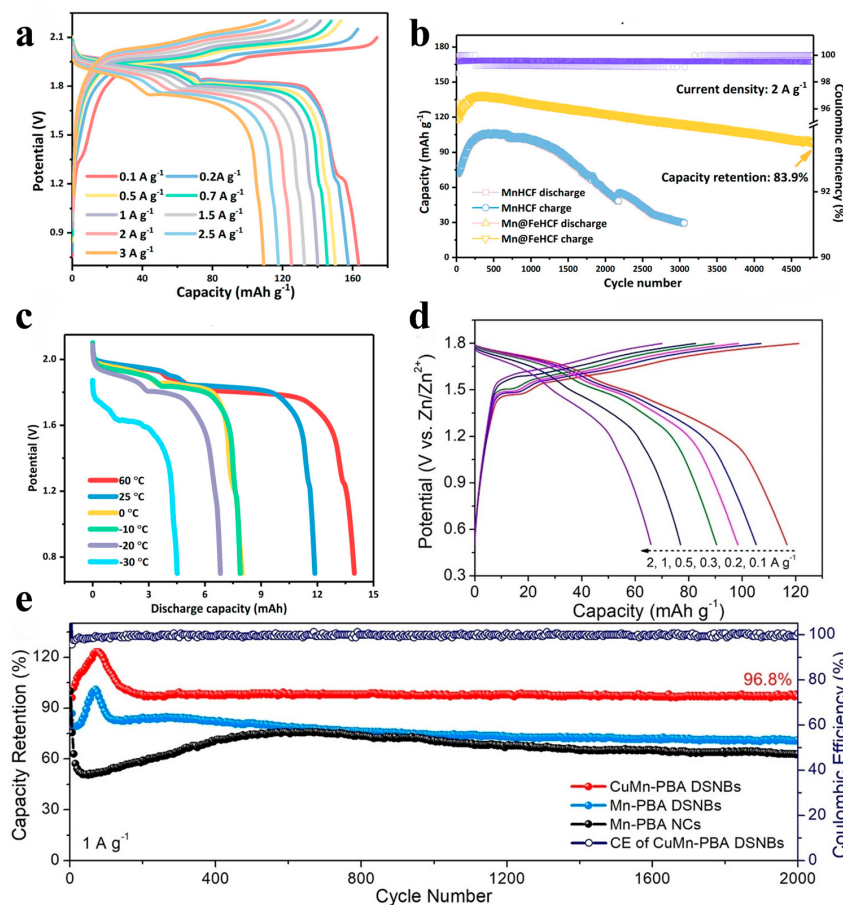


**Figure 8.** (a) Charge/discharge voltage profiles of  $Zn \parallel Mn@FeHCF$  cell. (b) Long-term cycling performance at  $2 \text{ A g}^{-1}$ . (c) Discharge voltage profiles of  $Zn \parallel Mn@FeHCF$  cell at  $0.03 \text{ A g}^{-1}$  under different temperatures. Reprinted with permission from ref. [45]. Copyright 2023, American Chemical Society. (d) Charge/discharge voltage profiles of the CuMn-PBA DSNB electrode at various current densities. (e) Cycling performance tested at  $1 \text{ A g}^{-1}$  of the Mn-PBA NC, Mn-PBA DSNB, and CuMn-PBA DSNB electrodes. Reprinted with permission from ref. [46]. Copyright 2022, John Wiley and Sons.

The challenge of the low loading of cathode materials in lightweight zinc-ion batteries necessitates the selection of cathode materials characterized by both high capacity and structural stability. Consequently, researchers have turned to manganese-based, vanadium-based, and Prussian blue analog materials. However, the performance of these materials is hindered by various factors. In the case of manganese-based materials, enhancing their performance can be achieved through modifications such as constructing composites, implementing defect engineering, and optimizing interfaces. Vanadium-based materials, on the other hand, can benefit from improved anode material performance by optimizing their structural morphology. As for Prussian blue analogs, altering the structure or introducing additional vacancies can lead to a notable increase in both the specific capacity and energy density of the anodes. These strategies underscore the importance of addressing material-specific challenges to unlock the full potential of these cathode materials in lightweight zinc-ion batteries.

#### 4. Design for Lightweight Separator

The electrolyte is a critical component in zinc-ion batteries, playing a pivotal role in influencing the electrochemical behavior and facilitating the transport of zinc ions between the positive and negative electrodes [47,48]. In the context of thin and lightweight zinc-ion batteries, the electrolyte must strike a balance between low weight and thickness, while also ensuring high ion transport rates and long service life. Typically, electrolytes are categorized as either liquid or gel forms.

Liquid electrolytes, in particular, are faced with the challenge of battery thickness being significantly impacted by the separator. However, using thin and lightweight separators can often result in battery damage due to insufficient mechanical properties and the accelerated growth of dendrites. To address this issue, the development of ultrathin and high-performance separators emerges as a strategic approach towards realizing thin and lightweight zinc-ion batteries. This innovative design not only enhances the overall performance of the battery but also mitigates the risks associated with traditional separator materials.

Li proposed an ultrathin separator with the functionality of actively stabilizing the zinc negative electrode (Figure 9a) [49]. The functional ultrathin separator was constructed by designing a C/Cu nanocomposite decorative layer on the ultrathin CNF membrane substrate. The CNF membrane substrate, prepared using a simple vacuum filtration method, exhibits high mechanical strength, a uniform nanoporous structure, and ion screening ability, which can effectively homogenize ion flux and enhance transfer rates during  $Zn^{2+}$  zinc deposition. Notably, the 20  $\mu m$  thick CNF membrane achieved an optimal balance between mechanical strength and ion transfer resistance, resulting in excellent dendrite resistance (Figure 9b,c). Fang fabricated PAN nanofiber films using an electrostatic spinning process [50]. The PAN separator exhibits exceptional pore connectivity, facilitating efficient ion transport (Figure 9d). With a thickness of 69  $\mu m$ , it is eight times thinner than the glass fiber (GF) separator (675  $\mu m$ ), thereby shortening the diffusion path length for zinc ions and improving AZIB's ion transport utilization efficiency. Moreover, the PAN separator demonstrates remarkable flexibility and tensile strength, enabling it to be bent at any desired angle.

Li fabricated a novel meso-bridged ultrathin (28.6  $\mu m$ ) polymer electrolyte (PSPZ) by employing electrostatic spinning to synthesize PAN nanofiber membranes, which were then combined with PEO/Zn(OTf)<sub>2</sub> electrolyte to form an interconnected 3D network (Figure 9e–h) [51]. Initially, thick and porous PAN/SiO<sub>2</sub> nanofiber membranes were prepared via electrostatic spinning. Subsequently, densification was achieved using a roller machine to reduce the thickness of the PAN/SiO<sub>2</sub> membrane and eliminate excessive interstitial space while maintaining good flexibility. The resulting membrane exhibited uniform distribution of fumed silica particles within it, with its average thickness reduced from 62.1  $\mu m$  to 13.3  $\mu m$  through rolling, thereby enhancing its mechanical strength.

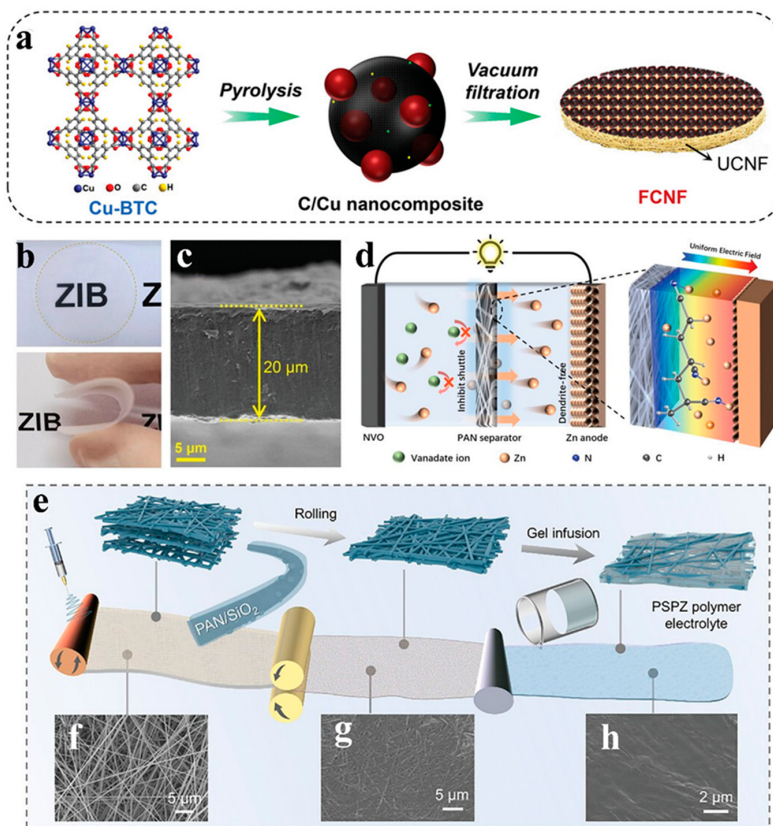


**Figure 9.** (a) Fabrication schematics of the double-layer functional ultrathin separators. (b) Photographs of the GF membrane; (c) cross-sectional SEM image. Reprinted with permission from ref. [49]. Copyright 2023, John Wiley and Sons. (d) The working mechanism of PAN separator in AZIBs. Reprinted with permission from ref. [50]. Copyright 2021, John Wiley and Sons. (e) Scheme diagram of mediator-bridged editing of polymer electrolyte, including a (f) digital photo of PAN/SiO<sub>2</sub> nanofiber membrane and field-emission scanning electron microscopy (FESEM) images of the (g) densified PAN/SiO<sub>2</sub> nanofiber membrane and (h) PSPZ polymer electrolyte. Reprinted with permission from ref. [51]. Copyright 2023, John Wiley and Sons.

Separators play a crucial role in zinc-ion batteries utilizing liquid electrolytes. However, the thickness of the separator plays a significant role in limiting the overall thinness of the battery. Separators that are too thin may suffer from inadequate mechanical strength. To address this challenge, researchers have developed ultrathin separators with high mechanical strength through various methods such as constructing a composite decorative layer, utilizing a robust biomass membrane, or employing electrostatic spinning techniques. These ultrathin separators not only meet the requirements for lightweight and thin batteries but also effectively inhibit adverse reactions at the zinc negative electrode. By enhancing the mechanical properties of the separator through innovative approaches, researchers have successfully optimized the performance of zinc-ion batteries while maintaining a thin and lightweight design.

### 5. Design for Lightweight Gel Electrolyte

Compared to liquid electrolytes, gel electrolytes offer superior corrosion resistance, precise regulation of zinc nucleation and growth, enhanced battery efficiency, excellent biocompatibility, improved ion transport rates, and increased chemical stability. Additionally, gel electrolytes effectively inhibit the water decomposition reaction. In the context of thin and lightweight zinc-ion batteries, the utilization of gel electrolytes can address issues such as liquid leakage resulting from misalignment, as well as minimize side reactions like hydrogen precipitation and corrosion in these portable devices.

Despite these advantages, challenges persist regarding the thickness and ionic conductivity of gel electrolytes when integrating them into thin and lightweight zinc-ion batteries. Achieving the optimal balance between these properties is essential for the successful incorporation of gel electrolytes into such battery designs.

### 5.1. Ultrathin Gel Electrolyte Design

Gel electrolytes combine the advantages of both liquid and solid electrolytes, enabling the rapid transfer of zinc ions and anions to improve the charging and discharging efficiency of batteries [52]. Furthermore, gel electrolytes help prevent solution loss during cycling, ultimately prolonging the battery's lifespan. The thickness of the gel electrolyte is crucial in determining the size of lightweight batteries. Thus, balancing the gel thickness with maintaining high ionic conductivity presents a significant challenge.

Tao's proposed approach for screen-printed organic-polymer electrolytes paves the way for ultrathin battery design (Figure 10a) [53]. This strategy employs a glycol-based organic-polymer electrolyte to enable the fabrication of flexible and printable zinc-ion thin-film batteries (Figure 10b). Not only is this gel electrolyte facile and cost-effective to prepare, but it also exhibits a high boiling point, thereby significantly enhancing battery safety. Compared to conventional aqueous electrolytes, the glycol-based polymeric electrolyte (PEL) effectively mitigated the issue of hydrogen precipitation in batteries, thereby enhancing battery efficiency and cycle life. In this study, self-supported zinc batteries with PEL printed electrodes demonstrated exceptional performance. The cell achieved an intermediate voltage of 1.35 V at a cutoff voltage of 2 V, exhibiting a stable voltage plateau. At a current density of  $0.5 \text{ mA cm}^{-2}$ , the cell exhibited an area capacity of  $4 \text{ mAh cm}^{-2}$ , which is sufficient for various low-power electronic devices. Moreover, the cell displayed excellent cycle stability with over 60 cycles at a current density of  $2 \text{ mA cm}^{-2}$ . Notably, the gel form of this polymeric electrolyte method exhibited remarkable printability by precisely controlling component ratios and curing time to achieve the desired viscosity and structural integrity during electrode screen printing. This feature simplifies the mass production process and eliminates the need for additional complex steps or synthesis methods, such as electrolyte injection or wetting.

Furthermore, Qu discovered that caffeine passivates the zinc anode and inhibits chemical corrosion [54]. Caffeine also coordinates with  $\text{Zn}^{2+}$  ions to form  $\text{Zn}^{2+}$  conductive complexes, which undergo conversion to  $\text{ZnCO}_3$  and  $2\text{ZnCO}_3 \cdot 3\text{Zn(OH)}_2$  during cycling. Consequently, these resulting Zn-rich interphase products significantly enhance the reversibility of zinc even at high utilization levels (Figure 10c,d). Caffeine was incorporated into a polyacrylamide hydrogel electrolyte and successfully patterned using photolithography techniques. Simultaneously, finger electrodes were fabricated comprising a collector (15 nm Cr and 60 nm Au) along with electrode materials. The self-rolling of the multilayer stack was achieved by incorporating an additional hydrogel layer with reduced swelling capacity, resulting in the assembly of microcells measuring 850  $\mu\text{m}$  in length and 160  $\mu\text{m}$  in diameter.

Similarly, Li successfully fabricated thin IL gels (approximately 500 nm thick) composed of a hydrophobic IL solvent, zinc salt, and thiolene polymer-compatible backbone (Figure 10e,f) [55]. These IL gels were prepared by spin-coating onto zinc electrodes followed by UV curing. The ultrathin IL gel effectively mitigated parasitic reactions such as electrolyte consumption and zinc anode corrosion while ensuring reliable zinc reversibility at a depth of discharge (DOD) of 90%. As a result of employing this thin IL gel, the assembled zinc-ion manganese-based full batteries exhibited exceptional charge/discharge cycling performance with a capacity retention rate of approximately 95.7% after undergoing 600 cycles.

However, the utilization of ultrathin gels often gives rise to issues such as cell breakage due to their inadequate mechanical properties. Hence, it is imperative to consider the mechanical characteristics of gels. Taking inspiration from reinforced concrete structures, Hu devised a pioneering nanofiber separator-gel composite electrolyte (Figure 10g) [56]. In this

case, the main chain of the thermoplastic polyurethane (TPU)-poly(mesitylene dicarboxamide) (PMIA) (TP for short) nanofiber separator enters the polyvinyl alcohol (PVA) gel. The TP fiber separator enhances the mechanical properties of the PTP composite gel electrolyte in order to accommodate the substantial volume variation at the electrode–electrolyte interface. Moreover, the intermolecular hydrogen bonding between the nanofiber separator and water reduced the number of water molecules involved in the HER, effectively suppressing dendrite formation and side reactions. Notably, the interaction between the TP nanofiber separator and PVA in the hybridized inner layer facilitated a fast  $Zn^{2+}$  migration pathway and promoted the desolvation of  $Zn^{2+}$ . The assembled symmetric cells demonstrated exceptional durability with 6500 h at 5  $mA\text{ cm}^{-2}$  and 5  $mAh\text{ cm}^{-2}$  as well as a capacity retention of 72.3% after 1500 cycles at 5  $A\text{ g}^{-1}$  for full cells.

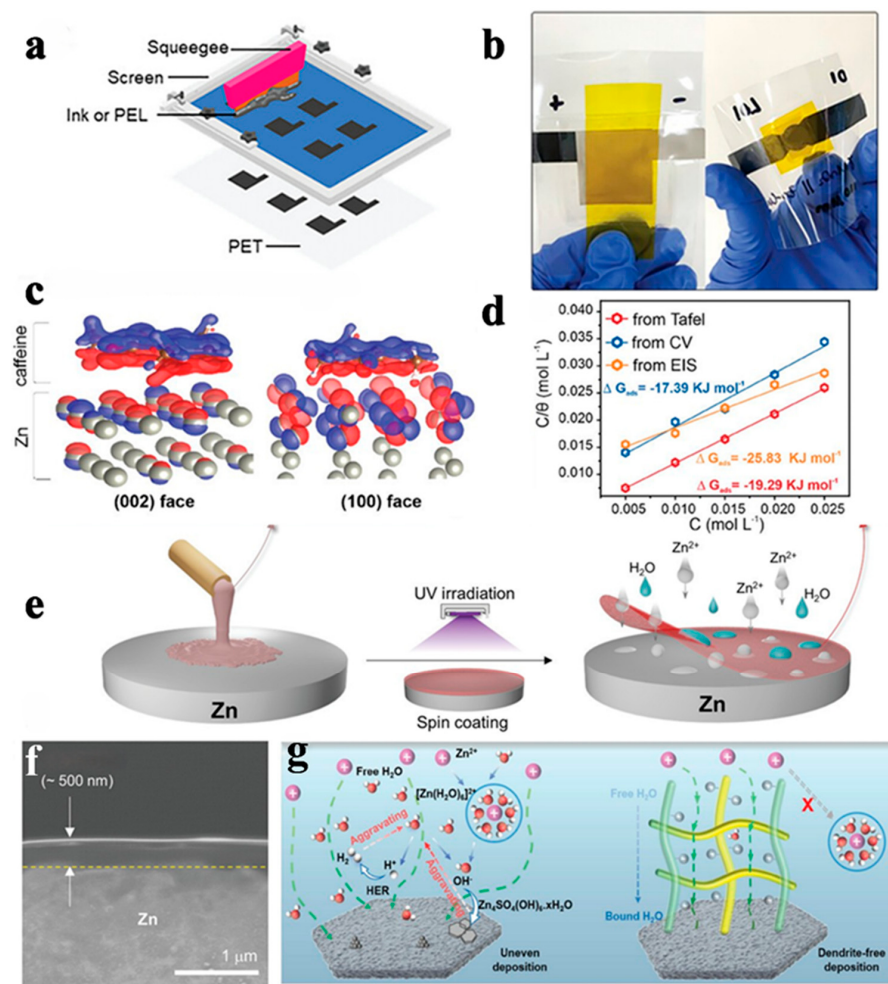


**Figure 10.** (a) Schematic illustration of the screen-printing process. (b) Photos of assembled screen-printed batteries. Reprinted with permission from ref. [53]. Copyright 2024, John Wiley and Sons. (c) Charge density distribution of caffeine on (002) and (100) face of metallic Zn. (d) Gibbs free energy of caffeine adsorption derived from Tafel plots, CV curves, and EIS spectra. Reprinted with permission from ref. [54]. Copyright 2024, John Wiley and Sons. (e) Depicting the fabrication of an IL skinny gel on a Zn anode. (f) Cross-sectional SEM image of the ILG-Zn. Reprinted with permission from ref. [55]. Copyright 2021, John Wiley and Sons. (g) Schematic illustration of ion migration channels of PTP. Reprinted with permission from ref. [56]. Copyright 2023, John Wiley and Sons.

### 5.2. In Situ-Polymerized Gel Electrolyte

By polymerizing the gel electrolyte *in situ* at the electrode, we can address the issues of suboptimal interfacial bonding and excessive free water molecules. This approach ensures a strong bond between the electrolyte and electrode, reducing the presence of free water

molecules that can hinder battery performance. The enhanced interfacial bond improves conductivity and helps prevent dendrite growth and side reactions, ultimately improving battery lifespan and safety.

Additionally, the *in situ*-polymerized gel electrolyte allows for a more integrated battery design, leading to thinner and lighter electrodes. This not only improves the overall performance of the battery but also contributes to its efficiency and portability. Overall, the *in situ* polymerization of gel electrolytes at the electrodes shows great promise for advancing battery technology and addressing key challenges in energy storage systems.

However, in order to achieve widespread application of *in situ*-polymerized gel electrolytes in batteries, several technical challenges must be addressed. These include precise control over the polymerization process of the gel electrolytes and ensuring uniform and stable interfacial bonding between the gel electrolytes and electrodes, as well as optimization of the ionic conduction properties. Researchers are required to execute a series of intricate chemical and physical processes under precisely controlled conditions to ensure the homogeneity and stability of the gel electrolyte. Wang skillfully employed the inorganic conductive layered material MXene and organic sodium polyacrylate (PAAS) as fundamental building blocks for the soft and hard phases, enabling the deposition of an organic–inorganic hybrid composite gel interfacial layer onto the surface of a zinc metal anode (Figure 11a,b) [57]. The combination of MXene’s inorganic conductivity and PAAS’s organic properties not only enhances the strength but also improves the toughness of the gel layer. This unique structural form and interfacial characteristics allow for high mechanical strength, excellent flexibility, and deformation ability of the composite gel, effectively preventing negative electrode structural damage and performance degradation during charge/discharge cycles.

Furthermore, the utilization of *in situ* growth technology facilitates a strong adhesion between the gel layer and the metal substrate, thereby not only reducing the battery’s dimensions but also augmenting the overall structural stability of the anode. Simultaneously, this *in situ*-grown gel layer effectively impedes dendrite growth and side reactions, consequently enhancing both the performance and reliability of the battery. Additionally, apart from surface deposition, Qin successfully fabricated a quasi-solid polymer gel electrolyte on zinc metal electrodes through *in situ* polymer redox polymerization techniques owing to their inherent reduction properties (Figure 11c) [58]. The proposed innovative strategy not only resolves the issue of the incompatible solid electrolyte–electrode interface in conventional batteries but also significantly enhances the performance of zinc-ion energy storage devices. By employing an *in situ* polymerization strategy, chemical stripping and polishing of the metal electrodes are achieved to establish a robust chemical bonding interaction between the electrodes and the electrolyte (Figure 11d). This chemical bonding interaction facilitates the formation of a strong bond between the solid-state metal electrode and quasi-solid-state gel electrolyte, effectively enhancing battery stability and cycle life. Importantly, this approach induces the optimal deposition of zinc along the (002) surface, thereby improving the reversibility and lifetime of the zinc negative electrode while mitigating zinc dendrite growth to prevent battery short-circuiting. The assembled battery achieves a stable cycle life of up to 5100 h and maintains stability for 240 h at ultra-high face capacity, while utilizing 87% of the zinc.

Furthermore, coupling agents play a crucial role in facilitating the combination of metals and gels. As chemical compounds that connect different materials and enhance interfacial bonding between them, coupling agents provide a stable connection between the metal electrode and gel electrolyte. Yang introduced a polyanion hydrogel film as a protective layer on the Zn anode with the assistance of a silane coupling agent [59]. Firstly, the silane coupling agent is advantageous due to its ability to establish connections between inorganic and organic interfaces, forming an organic matrix–silane coupling agent–inorganic matrix bonding layer (Figure 11e). The utilization of a silane coupling agent may assist in better adhesion of the polyanionic hydrogel film onto the Zn anode, resulting in the formation of a stable and uniform protective layer. The polyanionic hydrogel film

possesses functional groups within its hydrogel framework that facilitate the mineralization of  $\text{SO}_3^{2-}$ , thereby enabling a more uniform flux and transport of zinc ions. This characteristic enhances the performance and stability of the battery, preventing degradation caused by uneven ion distribution. Moreover, the chemically bonded hydrogel layer on the surface of zinc exhibits an anticatalytic effect, effectively inhibiting hydrogen precipitation and dendrite formation in zinc, thus crucially improving battery performance and safety. By employing this protective strategy using a polyanionic hydrogel film, Yang successfully achieved stable and reversible Zn stripping/plating at various currents and capacities. A remarkable full-cell capacity of 176  $\text{mAh g}^{-1}$  was attained with 4000 cycles at 10  $\text{A g}^{-1}$ . Li used this *in situ* polymerization gel approach and a simple and scalable transfer method to develop bifunctional battery and supercapacitor devices for skin-interfaced wearable electronics with thicknesses of less than 50  $\mu\text{m}$  (Figure 11f) [60] and supercapacitive and battery-type devices with a surface capacity of 113.4  $\text{mF cm}^{-2}$  and 6.1  $\mu\text{Ah cm}^{-2}$ . The exceptional flexibility of ultrathin energy devices enables excellent conformability to arbitrarily shaped surfaces, including elastic human skin, thereby augmenting the capabilities of inherently non-stretchable thin-film electronics.

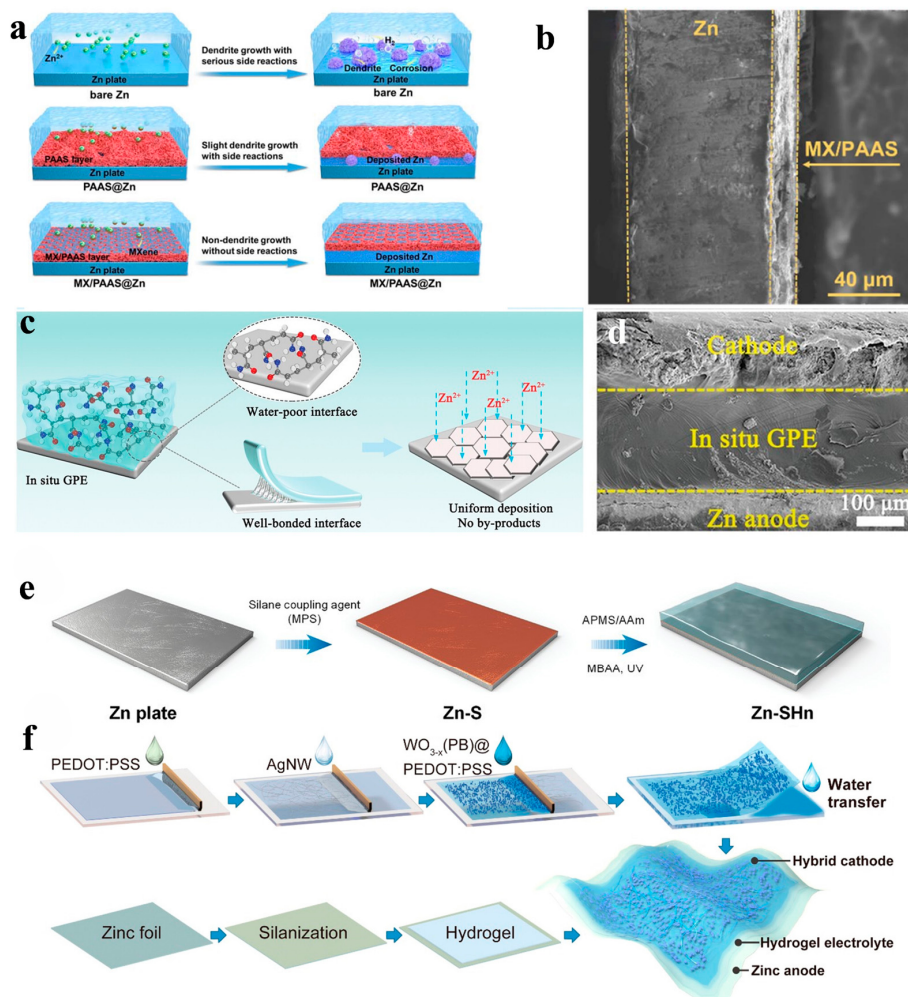


**Figure 11.** (a) Schematic diagram of zinc deposition on different electrodes. (b) SEM cross-section of treated electrode. Reprinted with permission from ref. [57]. Copyright 2024, American Chemical Society. (c) Schematic of in situ GPE at the electrode-electrolyte interface. (d) Cross-sectional SEM image of in situ ZHCs. Reprinted with permission from ref. [58]. Copyright 2022, John Wiley and Sons. (e) Schematic of the preparation of Zn-SHn. Reprinted with permission from ref. [59]. Copyright 2022, John Wiley and Sons. (f) Schematic of transfer printing process and device assembly. Reprinted with permission from ref. [60]. Copyright 2022, American Chemical Society.

The gel electrolyte used in lightweight zinc-ion batteries not only addresses the issue of liquid electrolyte leakage but also mitigates problems such as hydrogen precipitation and corrosion caused by traditional liquid electrolytes. This type of electrolyte can be broadly categorized into two main groups, with one being non-in situ-polymerized gels. To achieve a compact and lightweight design, researchers have focused on improving the production process and polymerization methods of these gels. Common approaches include screen printing organic polymer gels, photolithography, spin-coating, and creating separator-gel composite electrolytes.

However, non-in situ-polymerized gels may face challenges when in contact with the electrode, as the presence of water molecules between the two components can significantly impact the battery's cycling performance. In contrast, in situ-polymerized gels offer a solution to this issue, leading to improved battery efficiency and reduced size. Currently, enhancing the interfacial stability of in situ-polymerized gel electrolytes is a critical research focus. Researchers have explored various strategies, such as the precipitation of organic-inorganic hybrid composite gel interfacial layers, leveraging polymer redox reactions, and utilizing silane coupling agents to develop in situ polymerization gel electrolytes.

## 6. Design of Lightweight Zinc Battery Structures

The structural design of thin and lightweight zinc-ion batteries is crucial for enhancing battery performance, achieving slimness and lightness, and optimizing energy density [61]. Among these designs, the sandwich-type structure, planar-fork-finger-type structure, and integrated structure are commonly employed in thin and lightweight zinc-ion batteries [62,63]. The sandwich structure design typically involves the stacking of multiple layers of materials, with each layer serving a distinct function within the battery. This design offers the advantage of fully utilizing the properties of each layer to optimize cell performance. However, sandwich structures can present certain challenges, such as interfacial resistance between layers and stability issues. Conversely, the planar-fork-finger structural design adopts a unique geometry to enhance the contact area between the electrodes and electrolyte through the staggered arrangement of positive and negative electrodes, thereby increasing battery power density and energy density. This structural design facilitates battery thinness and lightness while improving overall performance. The one-piece structural design integrates all battery components into a continuous and seamless whole, simplifying the structure and minimizing the relative displacement or separation of components. Consequently, it ensures continuous and efficient ion and load transfer capability under complex deformation. Moreover, the integrated structural design contributes to both the structural and electrochemical stability of the cell, resulting in superior cell performance.

### 6.1. Sandwich-Type Battery

Sandwich structures are widely employed in commercial supercapacitors and batteries, making them the most prevalent choice. A typical sandwich structure comprises a cathode, an anode, and a quasi-solid electrolyte. By utilizing a robust packaging material and ensuring high-quality loading of the electrode active material, zinc-ion batteries with sandwich structures typically exhibit exceptional energy output. Zhou presents a wood-based AZIB with excellent flexibility (Figure 12a) [64]. Wood@Ni collectors were fabricated through chemical nickel plating on bleached wood, followed by Zn electrodeposition and  $\text{MnO}_2$  coating to obtain the anode and cathode, respectively (Figure 12b). Additionally, PAM/CNF/G hydrogel electrolytes were prepared using wood-derived CNF along with PAM and glycerol additives. By employing these components, sandwich-type zinc-ion batteries were assembled exhibiting remarkable operational stability and frost resistance (Figure 12c). Fu employed an autocatalytic nano-enhancement strategy to design a freeze-resistant and self-adhesive poly(amphiphilic ionic hydrogel) electrolyte (PZHE) (Figure 12d) [65]. Leveraging the gel's excellent electrical conductivity and robust interfacial adhesion, the sandwich-type zinc battery demonstrated a remarkable specific capacity of  $253 \text{ mAh g}^{-1}$ , along with exceptional cyclability and capacity retention. Moreover,

this battery exhibited outstanding performance even in low-temperature environments and under severe conditions such as bending (Figure 12e). Furthermore, the high-voltage platform offered by sandwich-type batteries represents a significant advantage. Liu proposed a zinc-ion aqueous hybrid battery utilizing an extensively concentrated bi-ionic electrolyte alongside a lithium-ion intercalated LiVPO<sub>4</sub>F cathode featuring a layered structure (Figure 12f) [66]. By formulating an enduring hydrogel electrolyte incorporating both a polymer hosting network and HCE, we successfully manufactured a flexible solid-state zinc hybrid battery. The exceptional flexibility and robustness exhibited by both the hydrogel electrolyte and electrodes bestowed remarkable stability and longevity upon our hybrid battery design. Furthermore, its flat high-voltage discharge platform renders it suitable for diverse applications in flexible devices, maintaining a stable output voltage of two series-connected cells at 3.7 V under 0.8 A g<sup>-1</sup> conditions (Figure 12g).

## 6.2. Flat-Fork-Finger Battery

The planar-fork-finger-type zinc-ion battery achieves a compact structural design by employing a staggered arrangement of the positive and negative electrodes in the form of planar fork fingers. This innovative design minimizes the internal space occupied by the battery, resulting in reduced size and weight while maintaining exceptional performance. Moreover, the planar-fork-finger structure significantly enhances the electrode–electrolyte contact area, thereby improving the electrochemical reaction efficiency and enabling higher energy storage within the same volume. Consequently, this advanced configuration allows for increased energy density without compromising on thinness or lightness, making it ideal for applications requiring prolonged operation. Wu developed a bipolar conformal strategy for the fabrication of a zinc negative electrode (rGO/PAM@Zn) with an interfacial protective layer structure by exploiting the spontaneous reaction between metallic zinc, graphene oxide (GO), and acrylamide (AM) (Figure 13a–c) [67]. This was coupled with a high-performance polypyrrole positive electrode (PPy/GO-AM). The resulting flexible zinc-ion capacitor demonstrated a surface capacitance of 125 mF cm<sup>-2</sup> and volumetric capacitance of 125 F cm<sup>-3</sup> at a current density of 1 mA cm<sup>-2</sup>, achieving an energy density of up to 44 µWh cm<sup>-2</sup>. Furthermore, it exhibited exceptional capacity retention of 90.3% after undergoing 5000 cycles. This bipolar conformal strategy presents a viable approach for designing and fabricating high-performance flexible zinc-based energy storage devices. In addition, when the battery pack consists of two flexible Zn-ion micro-supercapacitors (FZCs) connected in parallel, the discharge time is twice as long as that of a single FZC, which demonstrates the excellent homogeneity of the prepared FZCs. As a physical demonstration, two samples connected in series can drive a digital display, and the device works even in a highly bent state. These results demonstrate that the integrated FZCs have strong flexibility properties and have considerable potential for applications in flexible electronics (Figure 13d). In addition, Zhou reported the development of a high-performance planar quasi-solid-state zinc-ion metal battery (ZIMB) utilizing a vanadium-graphene (VG) film as an innovative interconnecting network to enhance the electrochemical performance of both the zinc anode and manganese dioxide cathode (Figure 13e) [68]. The VG film was initially introduced to improve the adhesion and charge transport capabilities of the active materials. The uniform electrodeposition of MnO<sub>2</sub> nanosheets and Zn nanosheets onto the highly conductive VG resulted in a MnO<sub>2</sub>@VG cathode and Zn@VG anode, respectively. The resulting Zn@VG // MnO<sub>2</sub>@VG fork-finger electrode configuration exhibited an exceptional areal capacity of 159 µAh cm<sup>-2</sup> at 0.05 mA cm<sup>-2</sup> with a remarkable Coulombic efficiency of 99.7%. The capacity retention ability of the assembled Zn@VG // MnO<sub>2</sub>@VG MBs under different bending angles with good flexibility meets the requirements of wearable devices (Figure 13f). Furthermore, it demonstrated superior areal energy / power density and excellent cycling stability. Wu developed a 3D network of MnO<sub>2</sub> electrodes with a thickness of up to 351 µm, which, owing to its porous structure and high hydrophilicity, enables the fabrication of a planar-fork-finger battery featuring an ultra-high surface capacity and power density zinc metal anode (Figure 13g) [69]. Lu utilized silver conductive ink printing

on cotton fabric as the collector for PZIMB (Figure 13h). Subsequently, P-NVO cathodic ink and Zn powder anodic ink were continuously printed onto the collector patterns to produce printed electrodes [70]. Finally, the prepared PAM-PVP hydrogel electrolyte film was applied to the printed electrodes to finalize the preparation of the PZIMB.

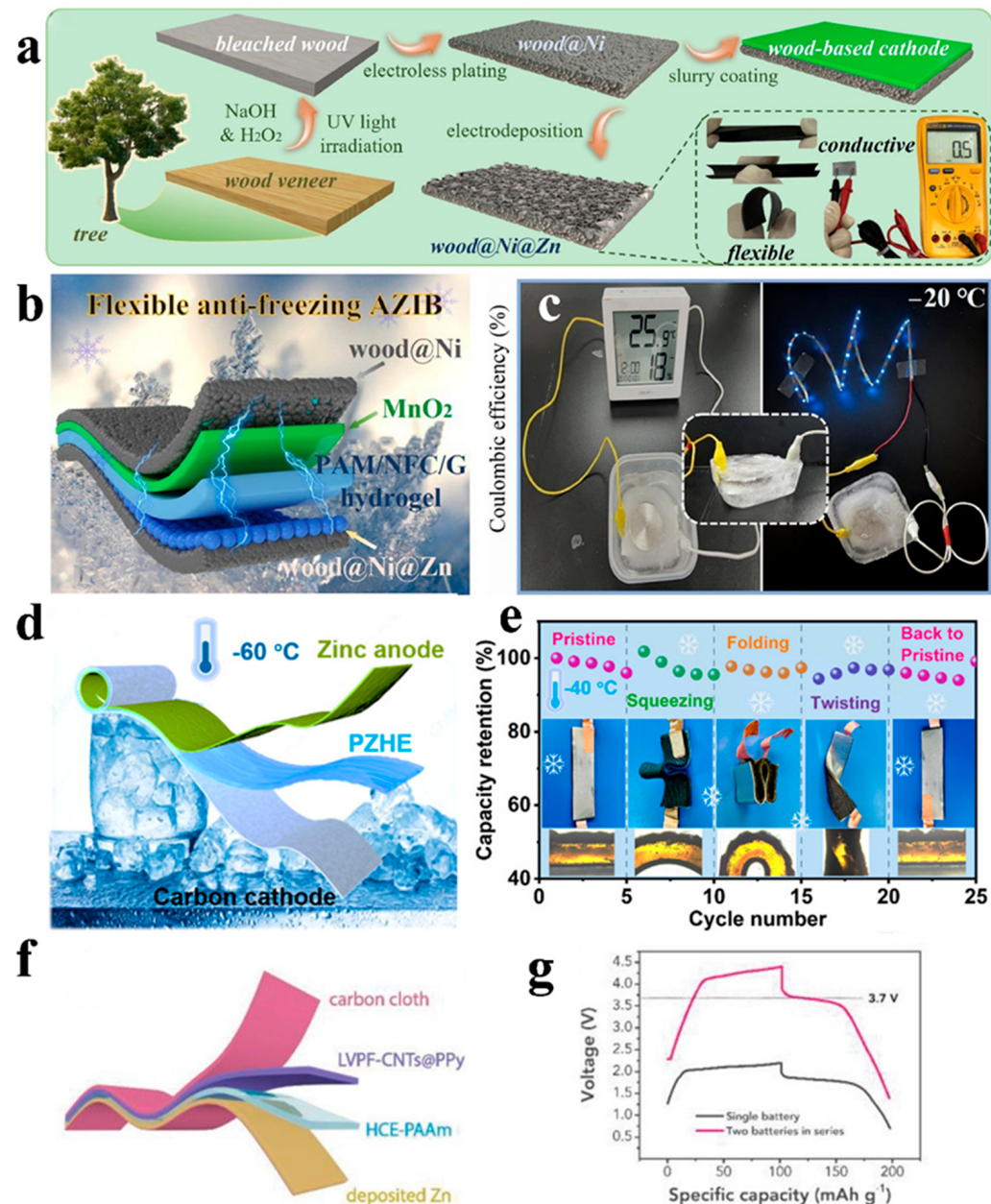


**Figure 12.** (a) Schematic illustration of the preparation of wood@Ni@Zn anode and wood-based cathode. (b) Schematic illustration of wood-based flexible anti-freezing AZIB. (c) Demonstrations of using one AZIB sealed in  $-20\text{ }^{\circ}\text{C}$  ice to power an electronic clock or a LED lamp belt. Reprinted with permission from ref. [64]. Copyright 2022, Elsevier. (d) Laminated structure of flexible ZIHCs. (e) Electrochemical performance of the flexible ZIHCs at  $5\text{ A g}^{-1}$  in squeezing, folding, and twisting. Reprinted with permission from ref. [65]. Copyright 2022, American Chemical Society. (f) Schematics of the configuration of the as-assembled flexible hybrid battery. (g) GCD curves of single zinc hybrid battery and the two zinc hybrid batteries connected in series at the current density of  $0.8\text{ A g}^{-1}$ . The latter serving as a watch belt yielded a stable output voltage of 3.7 V, corresponding to the working voltage of traditional LIBs. Reprinted with permission from ref. [66]. Copyright 2019, John Wiley and Sons.

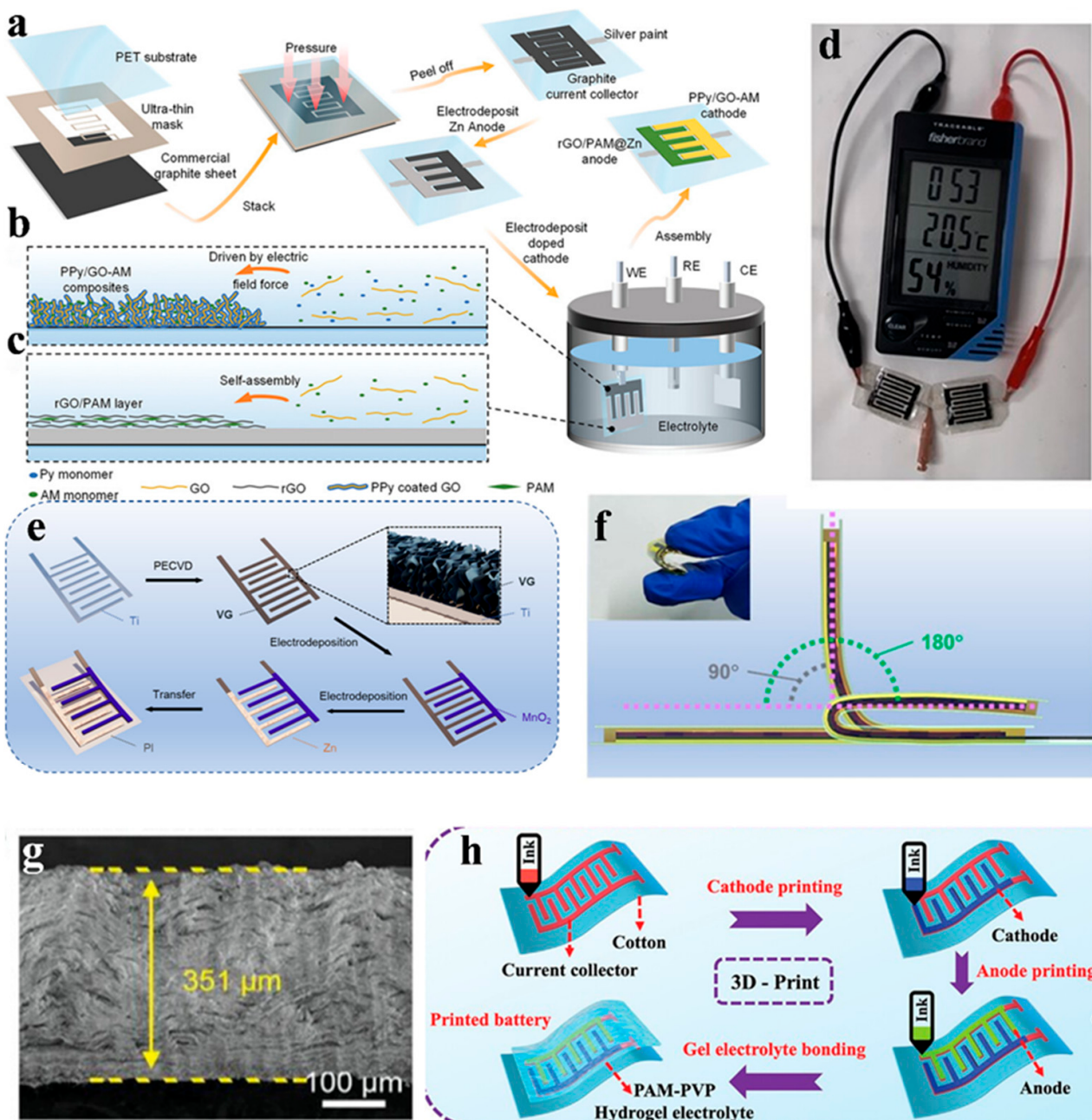


**Figure 13.** (a) Preparation process of FZCs. (b) Deposited PPy/GO-AM composites on GCC under electric field force. (c) Self-assembled rGO/PAM layer on GCC. (d) Photographs of two serial-connected FZCs powering a digital monitor. Reprinted with permission from ref. [67]. Copyright 2024, John Wiley and Sons. (e) Schematic illustration of the fabrication process of the interdigital Zn@VG // MnO<sub>2</sub>@VG electrode. (f) Photographs of flexible Zn@VG // MnO<sub>2</sub>@VG MBs. Reprinted with permission from ref. [68]. Copyright 2023, John Wiley and Sons. (g) Cross-sectional SEM images of the electrodes. Reprinted with permission from ref. [69]. Copyright 2023, John Wiley and Sons. (h) Schematic diagram of the 3D printing process. Reprinted with permission from ref. [70]. Copyright 2023, American Chemical Society.

### 6.3. Integrated Design Battery

The one-piece design facilitates a more compact integration of internal battery components, thereby minimizing unnecessary space and consequently enhancing the energy density of the battery. Simultaneously, this structural configuration also contributes to an im-

proved cycle life by ensuring sustained performance even after multiple charge/discharge cycles. Moreover, the integrated design mitigates potential issues such as relative displacement or separation commonly observed in conventional batteries, thus guaranteeing stable ion and electron transmission during charging and discharging processes. Consequently, this aids in reducing internal resistance while enhancing electrochemical stability under complex environmental conditions.

Yao reports on scalable and flexible ZIB all-in-one structures, which represent a remarkable breakthrough in the field of battery design (Figure 14a) [71]. They have successfully achieved an ultrathin all-in-one configuration by combining an innovative blade coating technique with a rolled assembly method (Figure 14b,c). This approach effectively overcomes the limitations associated with conventional coating or deposition methods in fabricating flexible zinc-based batteries. Notably, this technology not only enables precise control of electrode thickness but also enhances the ionic conductivity of composite electrodes, thereby significantly improving battery performance. In addition, due to the unique ultrathin integrated configuration, the resulting ZIB can be controllably customized and edited into arbitrary shapes and structures, extending its stretchable, editable, and customizable behavior and exhibiting excellent flexibility. Chen integrated the  $Zn(TfO)_2$ -PA protective coating between the Zn anode and the PA separator, acting as an adhesive to bond the Zn anode to the PA separator (Figure 14d) [72]. The cathode nanowires and multi-walled carbon nanotubes composed of  $\alpha\text{-MnO}_2$  are applied onto the separator using a conventional blade coating method, with the entire cathode layer serving as its own fluid collector (Figure 14e). In this resulting integrated configuration, there exist robust interfacial contacts facilitated by strong interactions among neighboring components. The integrated configuration not only enables the formation of dendrite-free and stable Zn anodes, leading to a longer cycle life compared to conventional loose stacked structures, but also enhances interfacial contact and reduces cell polarization, thereby improving multiplication capability. Moreover, the integrated configuration offers the possibility of replacing the metal collector with the cathode portion itself, resulting in a thinner and lighter battery. Additionally, robust interfacial bonding between neighboring components eliminates relative displacement or detachment during bending, ensuring the excellent flexibility and high strength required for flexible electronics (Figure 14f,g).

The sandwich design of zinc-ion batteries offers the potential for higher energy density through the efficient use of space. However, challenges arise when the device is bent, as this can cause components such as the separator, positive electrode, and negative electrode to displace or detach, resulting in increased contact resistance, blockage of electrical/ionic transport, and degradation of electrochemical performance.

On the other hand, the planar-fork-finger design enables the battery to conform to various planar shapes, making it well suited for applications in micro-robots, wearable sensors, and implantable medical devices. Moreover, the use of all-laser processing technology allows for the creation of high-precision electrode patterns, thereby increasing the electrochemical active sites of electrode materials and enhancing battery performance. However, this method comes at a high cost and may compromise the battery's ability to generate power from the back, impacting overall conversion efficiency. Furthermore, an integrated design approach consolidates all battery components into a seamless whole, ensuring continuous and effective interfacial connections that prevent component displacement or separation during complex deformations. This design also imparts high flexibility to the battery, enabling it to be cut and shaped according to specific requirements, thus expanding its versatility in terms of shape customization. Nonetheless, the complexity and stringent requirements of the preparation process pose challenges to implementation.

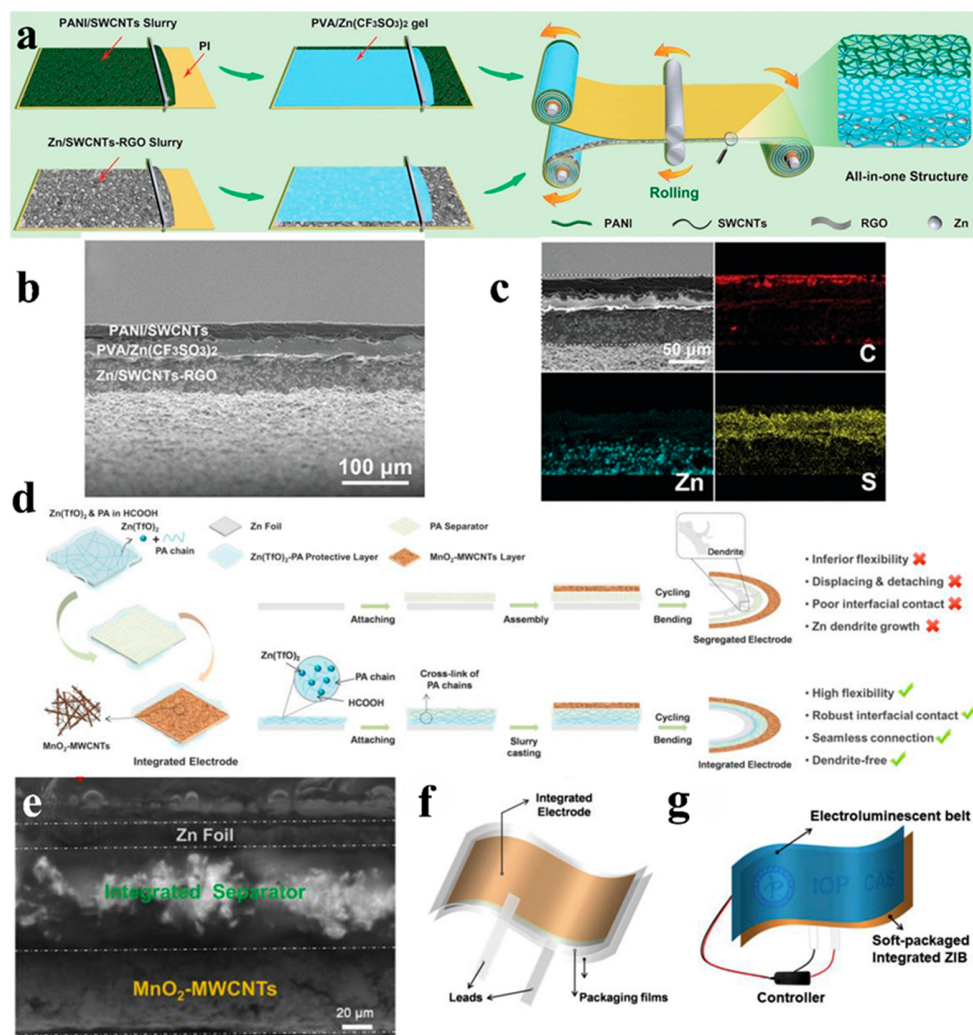


**Figure 14.** (a–c) The design of ultrathin all-in-one ZIBs: (a) schematic process, (b) cross-sectional SEM image, and (c) SEM elemental mappings. Reprinted with permission from ref. [71]. Copyright 2021, John Wiley and Sons. (d) Schematic illustration of the fabrication process of an integrated electrode as well as comparison of sections between the integrated electrode and segregated electrode. (e) SEM images of integrated electrode. (f) Schematic diagram of a soft-packaged integrated ZIB. (g) Schematic diagram of a flexible display unit using a flexible electroluminescent belt powered by soft-packaged integrated ZIBs. Reprinted with permission from ref. [72]. Copyright 2020, Elsevier.

## 7. Summary

As an emerging energy storage technology, lightweight zinc-ion batteries have demonstrated significant advancements in the domains of lightweight zinc anode and cathode design, separator and electrolyte formulation, and battery structure optimization. The rapid progress of this technology not only enhances the overall battery performance but also presents promising prospects for its application in wearable devices, mobile gadgets, and intelligent energy storage systems.

In terms of the design of thin and lightweight zinc anodes, researchers have made significant advancements in the design of thin and lightweight zinc anodes. Firstly, by optimizing the surface structure of the zinc anode, they have achieved a thinner and lighter anode, leading to a reduction in the overall weight and volume of the battery. This optimization has also improved the efficiency of zinc utilization within the anode. Secondly, through careful design of a zinc alloy layer, they have created a reliable substrate for the zinc battery, enhancing its cycling performance in terms of stability and durability.

Lastly, by integrating a microgrid structure into their design, researchers have managed to improve both the energy density and power density of these lightweight zinc-ion batteries significantly.

In terms of cathode material selection, researchers have endeavored to achieve exceptional electrochemical performance even at low loadings. As a result, the focus has been on identifying cathode materials with high capacity and structural stability. These materials primarily fall into three categories: manganese-based materials, vanadium-based materials, and Prussian blue analogs. However, the performance of these materials is influenced by various factors. To enhance the electrochemical properties of manganese-based materials, researchers have employed strategies such as constructing composites, implementing defect engineering, and optimizing interfaces. Vanadium-based materials have seen performance improvements through the optimization of their structural morphology. In the case of Prussian blue analogs, modifications to the structure or the introduction of additional vacancies have shown significant potential in enhancing the specific capacity and energy density of the cathode materials.

In terms of lightweight and thin separator design, researchers have made significant advancements in developing ultrathin separators with high mechanical strength using a variety of methods. These methods include constructing composite decorative layers, employing robust biomass membranes, and utilizing electrostatic spinning technology. These ultrathin separators not only fulfill the criteria for lightweight and thin batteries but also effectively prevent adverse reactions with zinc negative electrodes. Through the implementation of innovative techniques to enhance the mechanical properties of the separators, researchers have successfully optimized the performance of zinc-ion batteries while maintaining a lightweight and slim design.

In terms of lightweight gel design, gel electrolytes can be broadly classified into two main categories: non-in situ-polymerized gels and in situ-polymerized gels. For non-in situ-polymerized gels, researchers are focused on enhancing the production process and polymerization methods to achieve a compact and lightweight design. Common methods include screen-printed organic polymer gels, photolithography, spin-coating, and the fabrication of diaphragm-gel composite electrolytes. Significant progress has been made in reducing the thickness of these gels. However, challenges arise when these gels come into contact with electrodes, as the presence of water molecules between the components can negatively impact battery cycling performance. On the other hand, in situ-polymerized gels offer a solution to this challenge, leading to improved battery efficiency and reduced size. Research is currently centered on enhancing the interfacial stability of in situ-polymerized gel electrolytes. Various strategies have been explored, such as precipitating organic–inorganic hybrid composite gel interfacial layers, utilizing polymer redox reactions, and employing silane coupling agents in the development of in situ-polymerized gel electrolytes. Researchers have successfully decreased the thickness of gel electrolytes and achieved lightweight and slim designs.

In terms of the design of thin battery structures, researchers have explored innovative designs such as sandwich-type batteries, flat-fork-finger-type batteries, and integrated batteries. These designs effectively minimize inefficient space and reduce the weight within the battery. Consequently, this not only enhances the energy density and power density of the battery but also facilitates seamless integration into various devices.

Despite the significant advancements achieved in the performance and application of thin and lightweight zinc-ion batteries, several challenges still persist in their development. Firstly, there is a need to enhance the utilization rate of the zinc anode to attain high energy density in ultrathin batteries. Secondly, it is crucial to improve the water retention capability of thin and lightweight gels to enhance the cycle life of these batteries. Lastly, there is a requirement to design a battery structure that is more suitable for seamless integration with wearable devices while ensuring optimal user comfort. In the future, with the continuous advancement of materials science, nanotechnology, and battery manufacturing processes, there will be further enhancements in the performance of lightweight and thin

zinc-ion batteries. Researchers will persistently explore novel anode materials, electrolytes, and battery structures to overcome existing technological limitations. Simultaneously, as production costs decrease and commercialization progresses, these lightweight and thin zinc-ion batteries are anticipated to find widespread applications across various fields, thereby offering enhanced convenience and possibilities for people's lives.

**Author Contributions:** The manuscript was written through the contributions of all authors. All authors have read and agreed to the published version of the manuscript.

**Funding:** This work was supported by the National Natural Science Foundation of China (61904097).

**Conflicts of Interest:** The authors declare no conflicts of interest.

## References

1. Zhong, X.; Ye, S.; Tang, J.; Zhu, Y.; Wu, D.; Gu, M.; Pan, H.; Xu, B. Engineering Pt and Fe dual-metal single atoms anchored on nitrogen-doped carbon with high activity and durability towards oxygen reduction reaction for zinc-air battery. *Appl. Catal. B Environ.* **2021**, *286*, 119891. [[CrossRef](#)]
2. Huang, Y.; Ip, W.S.; Lau, Y.Y.; Sun, J.; Zeng, J.; Yeung, N.S.; Ng, W.S.; Li, H.; Pei, Z.; Xue, Q.; et al. Weavable, Conductive Yarn-Based NiCo<sub>x</sub>/Zn Textile Battery with High Energy Density and Rate Capability. *ACS Nano* **2017**, *11*, 8953–8961. [[CrossRef](#)] [[PubMed](#)]
3. Nakata, S.; Shiomi, M.; Fujita, Y.; Arie, T.; Akita, S.; Takei, K. A wearable pH sensor with high sensitivity based on a flexible charge-coupled device. *Nat. Electron.* **2018**, *1*, 596–603. [[CrossRef](#)]
4. Moin, A.; Zhou, A.; Rahimi, A.; Menon, A.; Benatti, S.; Alexandrov, G.; Tamakloe, S.; Ting, J.; Yamamoto, N.; Khan, Y.; et al. A wearable biosensing system with in-sensor adaptive machine learning for hand gesture recognition. *Nat. Electron.* **2021**, *4*, 54–63. [[CrossRef](#)]
5. Li, J.; Liu, Y.; Yuan, L.; Zhang, B.; Bishop, E.S.; Wang, K.; Tang, J.; Zheng, Y.Q.; Xu, W.; Niu, S.; et al. A tissue-like neurotransmitter sensor for the brain and gut. *Nature* **2022**, *606*, 94–101. [[CrossRef](#)] [[PubMed](#)]
6. Gao, W.; Emaminejad, S.; Nyein, H.Y.; Challa, S.; Chen, K.; Peck, A.; Fahad, H.M.; Ota, H.; Shiraki, H.; Kiriya, D.; et al. Fully integrated wearable sensor arrays for multiplexed in situ perspiration analysis. *Nature* **2016**, *529*, 509–514. [[CrossRef](#)] [[PubMed](#)]
7. Boto, E.; Holmes, N.; Leggett, J.; Roberts, G.; Shah, V.; Meyer, S.S.; Muñoz, L.D.; Mullinger, K.J.; Tierney, T.M.; Bestmann, S. Moving magnetoencephalography towards real-world applications with a wearable system. *Nature* **2018**, *555*, 657–661. [[CrossRef](#)] [[PubMed](#)]
8. Han, D.; Cui, C.; Zhang, K.; Wang, Z.; Gao, J.; Guo, Y.; Zhang, Z.; Wu, S.; Yin, L.; Weng, Z.; et al. A non-flammable hydrous organic electrolyte for sustainable zinc batteries. *Nat. Sustain.* **2022**, *5*, 205–213. [[CrossRef](#)]
9. Javed, M.S.; Mateen, A.; Ali, S.; Zhang, X.; Hussain, I.; Imran, M.; Shah, S.S.; Han, W. The emergence of 2D MXenes based Zn-ion batteries: Recent development and prospects. *Small* **2022**, *18*, 2201989. [[CrossRef](#)]
10. Yang, J.; Yin, B.; Sun, Y.; Pan, H.; Sun, W.; Jia, B.; Zhang, S.; Ma, T. Zinc anode for mild aqueous zinc-ion batteries: Challenges, strategies, and perspectives. *Nano-Micro Lett.* **2022**, *14*, 42. [[CrossRef](#)]
11. Zhai, S.; Jiang, Z.; Chen, X.; Hui, K.; Chen, F. Flexible one-dimensional Zn-based electrochemical energy storage devices: Recent progress and future perspectives. *J. Mater. Chem. A* **2021**, *9*, 26573–26602. [[CrossRef](#)]
12. Weng, G.; Yang, X.; Wang, Z.; Xu, Y.; Liu, R. Hydrogel Electrolyte Enabled High-Performance Flexible Aqueous Zinc Ion Energy Storage Systems toward Wearable Electronics. *Small* **2023**, *19*, 2303949. [[CrossRef](#)]
13. Yang, H.; Lee, J.; Cheong, J.Y.; Wang, Y.; Duan, G.; Hou, H.; Jiang, S.; Kim, I.-D. Molecular engineering of carbonyl organic electrodes for rechargeable metal-ion batteries: Fundamentals, recent advances, and challenges. *Energy Environ. Sci.* **2021**, *14*, 4228–4267. [[CrossRef](#)]
14. Li, C.; Jin, S.; Archer, L.A.; Nazar, L.F. Toward practical aqueous zinc-ion batteries for electrochemical energy storage. *Joule* **2022**, *6*, 1733–1738. [[CrossRef](#)]
15. Ruan, P.; Liang, S.; Lu, B.; Fan, H.J.; Zhou, J. Design strategies for high-energy-density aqueous zinc batteries. *Angewandte Chemie* **2022**, *134*, e202200598.
16. Shang, Y.; Kundu, D. A path forward for the translational development of aqueous zinc-ion batteries. *Joule* **2023**, *7*, 244–250. [[CrossRef](#)]
17. Zampardi, G.; La Mantia, F. Open challenges and good experimental practices in the research field of aqueous Zn-ion batteries. *Nat. Commun.* **2022**, *13*, 687. [[CrossRef](#)]
18. Zhu, Q.N.; Wang, Z.Y.; Wang, J.W.; Liu, X.Y.; Yang, D.; Cheng, L.W.; Tang, M.Y.; Qin, Y.; Wang, H. Challenges and strategies for ultrafast aqueous zinc-ion batteries. *Rare Met.* **2021**, *40*, 309–328. [[CrossRef](#)]
19. Deng, D.; Fu, K.; Yu, R.; Zhu, J.; Cai, H.; Zhang, X.; Wu, J.; Luo, W.; Mai, L. Ion tunnel matrix initiated oriented attachment for highly utilized Zn anodes. *Adv. Mater.* **2023**, *35*, 2302353. [[CrossRef](#)]
20. Wang, Z.; Zhou, M.; Qin, L.; Hu, A.; Meng, J.; Fu, Y.; Shi, Z. Simultaneous regulation of cations and anions in an electrolyte for high-capacity, high-stability aqueous zinc–vanadium batteries. *EScience* **2022**, *2*, 209–218. [[CrossRef](#)]

21. Choi, C.; Park, J.B.; Park, J.H.; Yu, S.; Kim, D.W. Simultaneous manipulation of electron/Zn<sup>2+</sup> ion flux and desolvation effect enabled by in-situ built ultra-thin oxide-based artificial interphase for controlled deposition of zinc metal anodes. *Chem. Eng. J.* **2023**, *456*, 141015. [[CrossRef](#)]
22. Zhang, L.; Zhang, B.; Zhang, T.; Li, T.; Shi, T.; Li, W.; Shen, T.; Huang, X.; Xu, J.; Zhang, X.; et al. Eliminating dendrites and side reactions via a multifunctional ZnSe protective layer toward advanced aqueous Zn metal batteries. *Adv. Funct. Mater.* **2021**, *31*, 2100186. [[CrossRef](#)]
23. Hao, J.; Li, B.; Li, X.; Zeng, X.; Zhang, S.; Yang, F.; Liu, S.; Li, D.; Wu, C.; Guo, Z. An In-Depth Study of Zn Metal Surface Chemistry for Advanced Aqueous Zn-Ion Batteries. *Adv. Mater.* **2020**, *32*, 2003021. [[CrossRef](#)]
24. Ling, W.; Nie, C.; Wu, X.; Zeng, X.X.; Mo, F.; Ma, Q.; Lu, Z.; Luo, G.; Huang, Y. Ion Sieve Interface Assisted Zinc Anode with High Zinc Utilization and Ultralong Cycle Life for 61 Wh/kg Mild Aqueous Pouch Battery. *ACS Nano* **2024**, *18*, 5003–5016. [[CrossRef](#)]
25. Zhou, S.; Wang, Y.; Lu, H.; Zhang, Y.; Fu, C.; Usman, I.; Liu, Z.; Feng, M.; Fang, G.; Cao, X.; et al. Anti-corrosive and Zn-ion-regulating composite interlayer enabling long-life Zn metal anodes. *Adv. Funct. Mater.* **2021**, *31*, 2104361. [[CrossRef](#)]
26. Zhou, J.; Xie, M.; Wu, F.; Mei, Y.; Hao, Y.; Huang, R.; Wei, G.; Liu, A.; Li, L.; Chen, R. Ultrathin Surface Coating of Nitrogen-Doped Graphene Enables Stable Zinc Anodes for Aqueous Zinc-Ion Batteries. *Adv. Mater.* **2021**, *33*, 2101649. [[CrossRef](#)]
27. Zhou, Y.; Xia, J.; Di, J.; Sun, Z.; Zhao, L.; Li, L.; Wu, Y.; Dong, L.; Wang, X.; Li, Q. Ultrahigh-Rate Zn Stripping and Plating by Capacitive Charge Carriers Enrichment Boosting Zn-Based Energy Storage. *Adv. Energy Mater.* **2023**, *13*, 2203165. [[CrossRef](#)]
28. Meng, Y.; Wang, L.; Zeng, J.; Hu, B.; Kang, J.; Zhang, Y.; Zhang, J.; Zhao, Z.; Zhang, L.; Lu, H. Ultrathin zinc-carbon composite anode enabled with unique three-dimensional interpenetrating structure for high-performance aqueous zinc ion batteries. *Chem. Eng. J.* **2023**, *474*, 145987. [[CrossRef](#)]
29. Li, R.; Du, Y.; Li, Y.; He, Z.; Dai, L.; Wang, L.; Wu, X.; Zhang, J.; Yi, J. Alloying Strategy for High-Performance Zinc Metal Anodes. *ACS Energy Lett.* **2023**, *8*, 457–476.
30. Fayette, M.; Chang, H.J.; Rodríguez-Pérez, I.A.; Li, X.; Reed, D. Electrodeposited zinc-based films as anodes for aqueous zinc batteries. *ACS Appl. Mater. Interfaces* **2020**, *12*, 42763–42772. [[CrossRef](#)]
31. Zhang, Q.; Luan, J.; Fu, L.; Wu, S.; Tang, Y.; Ji, X.; Wang, H. The Three-Dimensional Dendrite-Free Zinc Anode on a Copper Mesh with a Zinc-Oriented Polyacrylamide Electrolyte Additive. *Angew. Chem. Int. Ed.* **2019**, *58*, 15841–15847. [[CrossRef](#)]
32. Zhou, L.; Yang, F.; Zeng, S.; Gao, X.; Liu, X.; Gao, X.; Yu, P.; Lu, X. Zincophilic Cu Sites Induce Dendrite-Free Zn Anodes for Robust Alkaline/Neutral Aqueous Batteries. *Adv. Funct. Mater.* **2022**, *32*, 2110829. [[CrossRef](#)]
33. Li, Q.; Wang, H.; Yu, H.; Fu, M.; Liu, W.; Zhao, Q.; Huang, S.; Zhou, L.; Wei, W.; Ji, X.; et al. Engineering an Ultrathin and Hydrophobic Composite Zinc Anode with 24 μm Thickness for High-Performance Zn Batteries. *Adv. Funct. Mater.* **2023**, *33*, 2303466. [[CrossRef](#)]
34. Liu, H.; Li, J.; Zhang, X.; Liu, X.; Yan, Y.; Chen, F.; Zhang, G.; Duan, H. Ultrathin and Ultralight Zn Micromesh-Induced Spatial-Selection Deposition for Flexible High-Specific-Energy Zn-Ion Batteries. *Adv. Funct. Mater.* **2021**, *31*, 2106550. [[CrossRef](#)]
35. Wang, J.H.; Chen, L.F.; Dong, W.X.; Zhang, K.; Qu, Y.F.; Qian, J.W.; Yu, S.H. Three-Dimensional Zinc-Seeded Carbon Nanofiber Architectures as Lightweight and Flexible Hosts for a Highly Reversible Zinc Metal Anode. *ACS Nano* **2023**, *17*, 19087–19097. [[CrossRef](#)]
36. Chen, X.; Zhang, H.; Liu, J.H.; Gao, Y.; Cao, X.; Zhan, C.; Wang, Y.; Wang, S.; Chou, S.L.; Dou, S.X.; et al. Vanadium-based cathodes for aqueous zinc-ion batteries: Mechanism, design strategies and challenges. *Energy Storage Mater.* **2022**, *50*, 21–46. [[CrossRef](#)]
37. Cui, J.; Guo, Z.; Yi, J.; Liu, X.; Wu, K.; Liang, P.; Li, Q.; Liu, Y.; Wang, Y.; Xia, Y.; et al. Organic cathode materials for rechargeable zinc batteries: Mechanisms, challenges, and perspectives. *ChemSusChem* **2020**, *13*, 2160–2185. [[CrossRef](#)]
38. Li, G.; Sun, L.; Zhang, S.; Zhang, C.; Jin, H.; Davey, K.; Liang, G.; Liu, S.; Mao, J.; Guo, Z. Developing cathode materials for aqueous zinc ion batteries: Challenges and practical prospects. *Adv. Funct. Mater.* **2024**, *34*, 2301291. [[CrossRef](#)]
39. Wu, B.; Zhang, G.; Yan, M.; Xiong, T.; He, P.; He, L.; Xu, X.; Mai, L. Graphene scroll-coated α-MnO<sub>2</sub> nanowires as high-performance cathode materials for aqueous Zn-ion battery. *Small* **2018**, *14*, 1703850. [[CrossRef](#)]
40. Ding, S.; Zhang, M.; Qin, R.; Fang, J.; Ren, H.; Yi, H.; Liu, L.; Zhao, W.; Li, Y.; Yao, L.; et al. Oxygen-deficient β-MnO<sub>2</sub>@graphene oxide cathode for high-rate and long-life aqueous zinc ion batteries. *Nano-Micro Lett.* **2021**, *13*, 173. [[CrossRef](#)]
41. Li, W.; Wang, D. Conversion-Type Cathode Materials for Aqueous Zn Metal Batteries in Nonalkaline Aqueous Electrolytes: Progress, Challenges, and Solutions. *Adv. Mater.* **2023**, *2304983*. [[CrossRef](#)]
42. Gao, W.; Michalička, J.; Pumera, M. Hierarchical atomic layer deposited V<sub>2</sub>O<sub>5</sub> on 3D printed nanocarbon electrodes for high-performance aqueous zinc-ion batteries. *Small* **2022**, *18*, 2105572. [[CrossRef](#)]
43. Wang, T.; Li, S.; Weng, X.; Gao, L.; Yan, Y.; Zhang, N.; Qu, X.; Jiao, L.; Liu, Y. Ultrafast 3D Hybrid-Ion Transport in Porous V<sub>2</sub>O<sub>5</sub> Cathodes for Superior-Rate Rechargeable Aqueous Zinc Batteries. *Adv. Energy Mater.* **2023**, *13*, 2204358. [[CrossRef](#)]
44. Zong, Q.; Wu, Y.; Liu, C.; Wang, Q.; Zhuang, Y.; Wang, J.; Tao, D.; Zhang, Q.; Cao, G. Tailoring layered transition metal compounds for high-performance aqueous zinc-ion batteries. *Energy Storage Mater.* **2022**, *52*, 250–283. [[CrossRef](#)]
45. Yang, G.; Liang, Z.; Li, Q.; Li, Y.; Tian, F.; Wang, C. Epitaxial Core–Shell MnFe Prussian Blue Cathode for Highly Stable Aqueous Zinc Batteries. *ACS Energy Lett.* **2023**, *8*, 4085–4095. [[CrossRef](#)]
46. Zeng, Y.; Xu, J.; Wang, Y.; Li, S.; Luan, D.; Lou, X.W. Formation of CuMn Prussian Blue Analog Double-Shelled Nanoboxes Toward Long-Life Zn-ion Batteries. *Angew. Int. Ed.* **2022**, *61*, e202212031. [[CrossRef](#)]
47. Wang, W.; Li, C.; Liu, S.; Zhang, J.; Zhang, D.; Du, J.; Zhang, Q.; Yao, Y. Flexible Quasi-Solid-State Aqueous Zinc-Ion Batteries: Design Principles, Functionalization Strategies, and Applications. *Adv. Energy Mater.* **2023**, *13*, 2300250. [[CrossRef](#)]

48. Pan, Z.; Yang, J.; Jiang, J.; Qiu, Y.; Wang, J. Flexible quasi-solid-state aqueous Zn-based batteries: Rational electrode designs for high-performance and mechanical flexibility. *Mater. Today Energy* **2020**, *18*, 100523. [[CrossRef](#)]
49. Li, Y.; Peng, X.; Li, X.; Duan, H.; Xie, S.; Dong, L.; Kang, F. Functional Ultrathin Separators Proactively Stabilizing Zinc Anodes for Zinc-Based Energy Storage. *Adv. Mater.* **2023**, *35*, 2300019. [[CrossRef](#)]
50. Fang, Y.; Xie, X.; Zhang, B.; Chai, Y.; Lu, B.; Liu, M.; Zhou, J.; Liang, S. Regulating Zinc Deposition Behaviors by the Conditioner of PAN Separator for Zinc-Ion Batteries. *Adv. Funct. Mater.* **2022**, *32*, 2109671. [[CrossRef](#)]
51. Li, Y.; Yang, X.; He, Y.; Li, F.; Ouyang, K.; Ma, D.; Feng, J.; Huang, J.; Zhao, J.; Yang, M.; et al. A Novel Ultrathin Multiple-Kinetics-Enhanced Polymer Electrolyte Editing Enabled Wide-Temperature Fast-Charging Solid-State Zinc Metal Batteries. *Adv. Funct. Mater.* **2024**, *34*, 2307736. [[CrossRef](#)]
52. Liu, D.; Tang, Z.; Luo, L.; Yang, W.; Liu, Y.; Shen, Z.; Fan, X.-H. Self-healing solid polymer electrolyte with high ion conductivity and super stretchability for all-solid zinc-ion batteries. *ACS Appl. Mater. Interfaces* **2021**, *13*, 36320–36329. [[CrossRef](#)]
53. Tao, S.; Ramirez, J.; Shewan, H.M.; Lyu, M.; Gentle, I.; Wang, L.; Knibbe, R. Ink to Power: An Organic-based Polymer Electrolyte for Ambient Printing of Flexible Zinc Batteries. *Adv. Funct. Mater.* **2024**, *24*, 2402050. [[CrossRef](#)]
54. Qu, Z.; Ma, J.; Huang, Y.; Li, T.; Tang, H.; Wang, X.; Liu, S.; Zhang, K.; Lu, J.; Karnaushenko, D.D.; et al. A Photolithographable Electrolyte for Deeply Rechargeable Zn Microbatteries in On-Chip Devices. *Adv. Mater.* **2024**, *36*, 2310667. [[CrossRef](#)]
55. Lee, D.; Kim, H.I.; Kim, W.Y.; Cho, S.K.; Baek, K.; Jeong, K.; Ahn, D.B.; Park, S.; Kang, S.J.; Lee, S.Y. Water-Repellent Ionic Liquid Skinny Gels Customized for Aqueous Zn-Ion Battery Anodes. *Adv. Funct. Mater.* **2021**, *31*, 2103850. [[CrossRef](#)]
56. Hu, W.; Zhang, Y.; Ju, J.; Wang, Y.; Zhang, Z.; Kang, W. Nanofiber-Reinforced Composite Gel Enabling High Ionic Conductivity and Ultralong Cycle Life for Zn Ion Batteries. *Small* **2024**, *20*, 2305140. [[CrossRef](#)]
57. Wang, J.; Zou, X.; Song, L.; Hou, Y.; Lu, J.; Gao, X.; He, Q.; Ren, Y.; Zhan, X.; Zhang, Q. A bio-inspired multifunctional interface layer for high performance zinc-ion batteries via novel in situ electropolymerization. *J. Mater. Chem. A* **2023**, *11*, 23973–23983. [[CrossRef](#)]
58. Qin, Y.; Li, H.; Han, C.; Mo, F.; Wang, X. Chemical Welding of the Electrode–Electrolyte Interface by Zn-Metal-Initiated In Situ Gelation for Ultralong-Life Zn-Ion Batteries. *Adv. Mater.* **2022**, *34*, 2207118. [[CrossRef](#)]
59. Yang, J.L.; Li, J.; Zhao, J.W.; Liu, K.; Yang, P.; Fan, H.J. Stable Zinc Anodes Enabled by a Zincophilic Polyanionic Hydrogel Layer. *Adv. Mater.* **2022**, *34*, 2202382. [[CrossRef](#)]
60. Li, J.; Yang, P.; Li, X.; Jiang, C.; Yun, J.; Yan, W.; Liu, K.; Fan, H.J.; Lee, S.W. Ultrathin Smart Energy-Storage Devices for Skin-Interfaced Wearable Electronics. *ACS Energy Lett.* **2023**, *8*, 1–8. [[CrossRef](#)]
61. Li, C.; Li, L.; He, B.; Ling, Y.; Pu, J.; Wei, L.; Sun, L.; Zhang, Q.; Yao, Y. Roadmap for flexible solid-state aqueous batteries: From materials engineering and architectures design to mechanical characterizations. *Mater. Sci. Eng. R Rep.* **2022**, *148*, 100671. [[CrossRef](#)]
62. Xiong, C.; Wang, T.; Zhou, L.; Zhang, Y.; Dai, L.; Zhou, Q.; Ni, Y. Fabrication of dual-function conductive cellulose-based composites with layered conductive network structures for supercapacitors and electromagnetic shielding. *Chem. Eng. J.* **2023**, *472*, 144958. [[CrossRef](#)]
63. Xiong, C.; Zheng, C.; Zhang, Z.; Xiong, Q.; Zhou, Q.; Li, D.; Shen, M.; Ni, Y. Polyaniline@ cellulose nanofibers multifunctional composite material for supercapacitors, electromagnetic interference shielding and sensing. *J. Mater.* **2024**, *in press*. [[CrossRef](#)]
64. Zhou, W.; Wu, T.; Chen, M.; Tian, Q.; Han, X.; Xu, X.; Chen, J. Wood-based electrodes enabling stable, anti-freezing, and flexible aqueous zinc-ion batteries. *Energy Storage Mater.* **2022**, *51*, 286–293. [[CrossRef](#)]
65. Fu, Q.; Hao, S.; Meng, L.; Xu, F.; Yang, J. Engineering Self-Adhesive Polyzwitterionic Hydrogels for Flexible Zinc-Ion Hybrid Capacitors with Superior Low-Temperature Adaptability. *ACS Nano* **2021**, *15*, 18469–18482. [[CrossRef](#)]
66. Liu, Z.; Yang, Q.; Wang, D.; Liang, G.; Zhu, Y.; Mo, F.; Huang, Z.; Li, X.; Ma, L.; Tang, T.; et al. A Flexible Solid-State Aqueous Zinc Hybrid Battery with Flat and High-Voltage Discharge Plateau. *Adv. Energy Mater.* **2019**, *9*, 1902473. [[CrossRef](#)]
67. Wu, Y.; Yuan, W.; Wang, P.; Wu, X.; Chen, J.; Shi, Y.; Ma, Q.; Dan, L.U.; Chen, Z.; Yu, A. Conformal Engineering of Both Electrodes Toward High-Performance Flexible Quasi-Solid-State Zn-Ion Micro-Supercapacitors. *Adv. Sci.* **2024**, *2308021*. [[CrossRef](#)]
68. Zhou, Y.; Li, W.; Xie, Y.; Deng, L.; Ke, B.; Jian, Y.; Cheng, S.; Qu, B.; Wang, X. Vertical Graphene Film Enables High-Performance Quasi-Solid-State Planar Zinc-Ion Microbatteries. *ACS Appl. Mater. Interfaces* **2023**, *15*, 9486–9493. [[CrossRef](#)]
69. Wu, Y.; He, N.; Liang, G.; Zhang, C.; Liang, C.; Ho, D.; Wu, M.; Hu, H. Thick-Network Electrode: Enabling Dual Working Voltage Plateaus of Zn-ion Micro-Battery with Ultrahigh Areal Capacity. *Adv. Funct. Mater.* **2024**, *34*, 2301734. [[CrossRef](#)]
70. Lu, Y.; Wang, Z.; Li, M.; Li, Z.; Hu, X.; Xu, Q.; Wang, Y.; Liu, H.; Wang, Y. 3D Printed Flexible Zinc Ion Micro-Batteries with High Areal Capacity Toward Practical Application. *Adv. Funct. Mater.* **2024**, *34*, 2310966. [[CrossRef](#)]
71. Yao, M.; Yuan, Z.; Li, S.; He, T.; Wang, R.; Yuan, M.; Niu, Z. Scalable Assembly of Flexible Ultrathin All-in-One Zinc-Ion Batteries with Highly Stretchable, Editable, and Customizable Functions. *Adv. Mater.* **2021**, *33*, 2008140. [[CrossRef](#)] [[PubMed](#)]
72. Chen, P.; Zhou, W.; Xiao, Z.; Li, S.; Wang, Z.; Wang, Y.; Xie, S. An integrated configuration with robust interfacial contact for durable and flexible zinc ion batteries. *Nano Energy* **2020**, *74*, 104905. [[CrossRef](#)]